

# GroupMeeting

2020.1.6

张慕琪

# Papers

1. Bias correction and downscaling of future RCM precipitation projection using a MOS-Analog technique. M. Turco, M.C. Llasat, S. Herrera, and J.M. Guitierrez. AGU Publications , 1 Feb 2017. 西班牙
2. Bias Correction, Quantile Mapping, and Downscaling: Revising the Inflation Issue. Douglas Maraun. 7 January 2013. 德国
3. Stactitical downscaling of general circulation model outputs to precipitation - part1: calibration and validation. D.A. Sachinara, F. Huang, A. Barton, and B.J.C. Perera. International Journal of Climatology, Royal Meteorological Society. 20 January 2014 in Wiley Online Library. 澳大利亚



JGR

A purple semi-circular graphic with the letters "JGR" in white, positioned above a white swoosh graphic.

## Journal of Geophysical Research: Atmospheres

### RESEARCH ARTICLE

10.1002/2016JD025724

### Bias correction and downscaling of future RCM precipitation projections using a MOS-Analog technique

M. Turco<sup>1,2</sup> , M. C. Llasat<sup>1</sup> , S. Herrera<sup>3</sup> , and J. M. Gutiérrez<sup>4</sup> 

<sup>1</sup>Department of Applied Physics, University of Barcelona (UB), Barcelona, Spain, <sup>2</sup>Barcelona Supercomputing Center (BSC), Barcelona, Spain, <sup>3</sup>Meteorology Group, Department of Applied Mathematics and Computer Science, Universidad de Cantabria, Santander, Spain, <sup>4</sup>Meteorology Group, Instituto de Física de Cantabria, CSIC-Universidad de Cantabria, Santander, Spain

# Introduction

降水变量是对于很多领域都具有重要的研究意义的变量，例如农业、水文，特别是对包含了极端事件的应用或气候变化来讲。

降尺度方法可以提高降水变量的空间尺度精度。

然而，降尺度后的模型依旧有较大的偏差；对此，模式输出统计(Model Output Statistics)方法使用的最为广泛。

# Introduction

## Climate Change Studies

distribution-wise

修正方程由观测和模拟的分布决定  
(即包含了分位数映射的偏差校正)

MOS-Analog

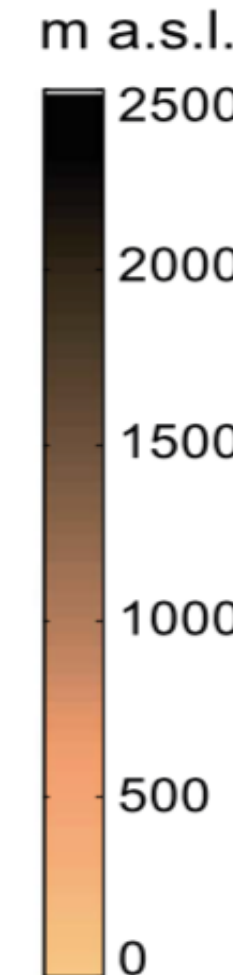
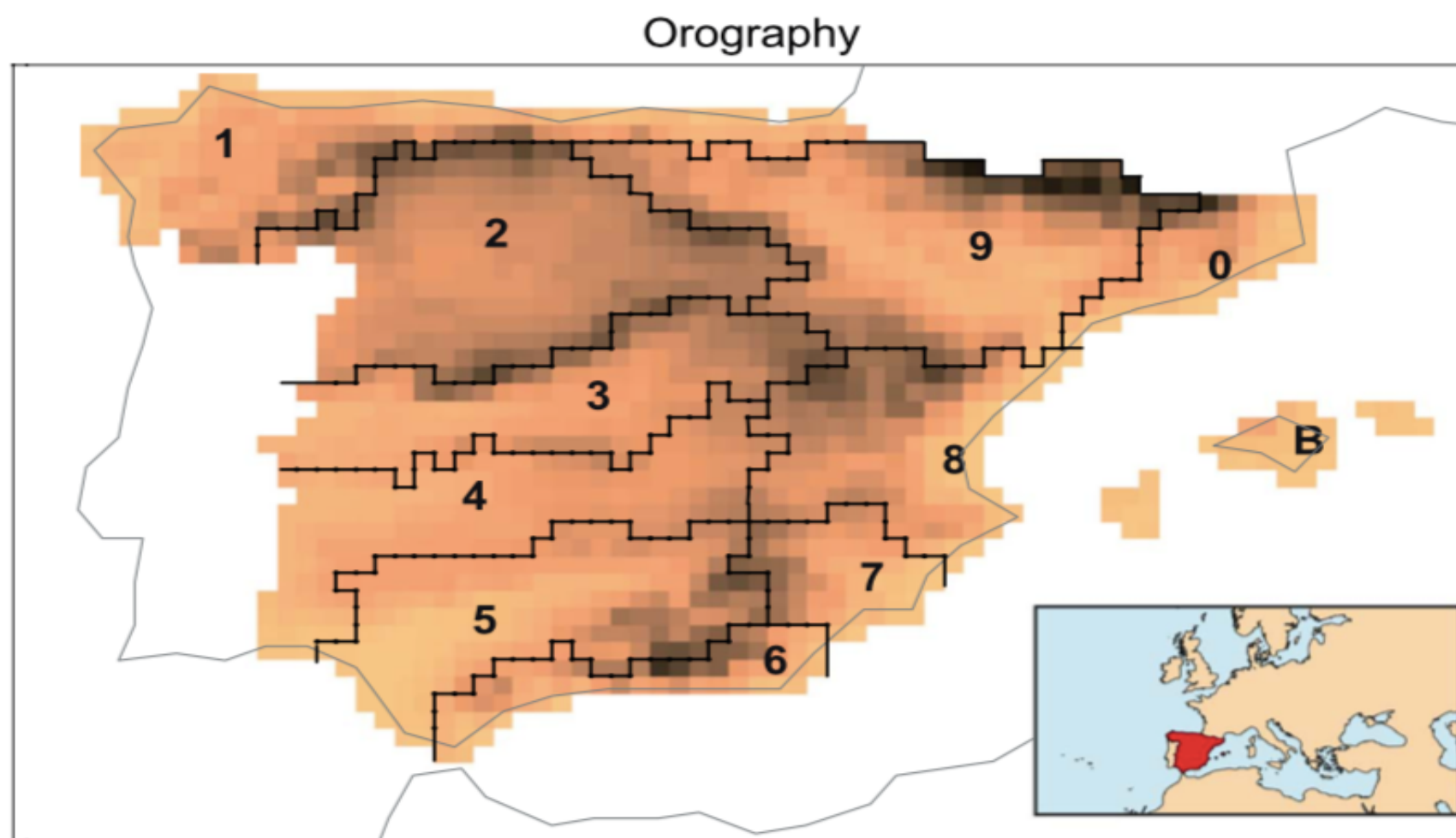
- 1) QQM会改变原始的气候变化信号
- 2) QQM无法矫正模型在大尺度环流上产生的误差
- 3) 由于RCM输出和观测具有不同的分辨率, QQM是低效的

event-wise

使用模拟和观测间的空间相似性

- 1) 概念上更简单、成本低
- 2) 可以重现预报因子和预报量间的非线性关系
- 3) 可以真实的再现空间上的降水特征,  
但无法模拟未观测到(unobserved)的天气特征

# Method



地形复杂且多样；  
由于处于不同气候  
地区，因此其气候  
变化大。  
(EAR40驱动的  
RCM模拟可以捕  
捉到该地区不同流  
域的年循环)

**Figure 1.** Topography of Spanish Iberian Peninsula and the Balearic Islands as represented by Spain02 at  $0.2^\circ \times 0.2^\circ$ , showing the main river basins: (0) Catalana, (1) Norte, (2) Duero, (3) Tajo, (4) Guadiana, (5) Guadalquivir, (6) Sur, (7) Segura, (8) Levante, (9) Ebro, and (B) Baleares. The inset shows a geographical map at larger scale.

## 1. ENSEMBLES RCM Data set

EU-funded project ENSEMBLES是欧洲各个国家共同合作，覆盖整个欧洲的数据集

## 2. Observed Data

高分辨率的Spain02( $0.2^\circ \times 0.2^\circ$ ,  $20 \text{ km} \times 20 \text{ km}$  approximately) data set

# Method

## 1. MOS-Analog downscaling

- 1) 对于每个由GCM驱动的RCM模拟的降水数值 $A(t)$ ，通过两个数据的欧几里得距离，可以获得 $t'$ 时刻，由ERA40驱动的RCM模拟的降水数值 $B(t')$ ；
- 2) 同样，在 $t'$ 时刻得到的观测降水数值 $b(t')$ 被作为降尺度的数据分配给由GCM驱动的RCM。

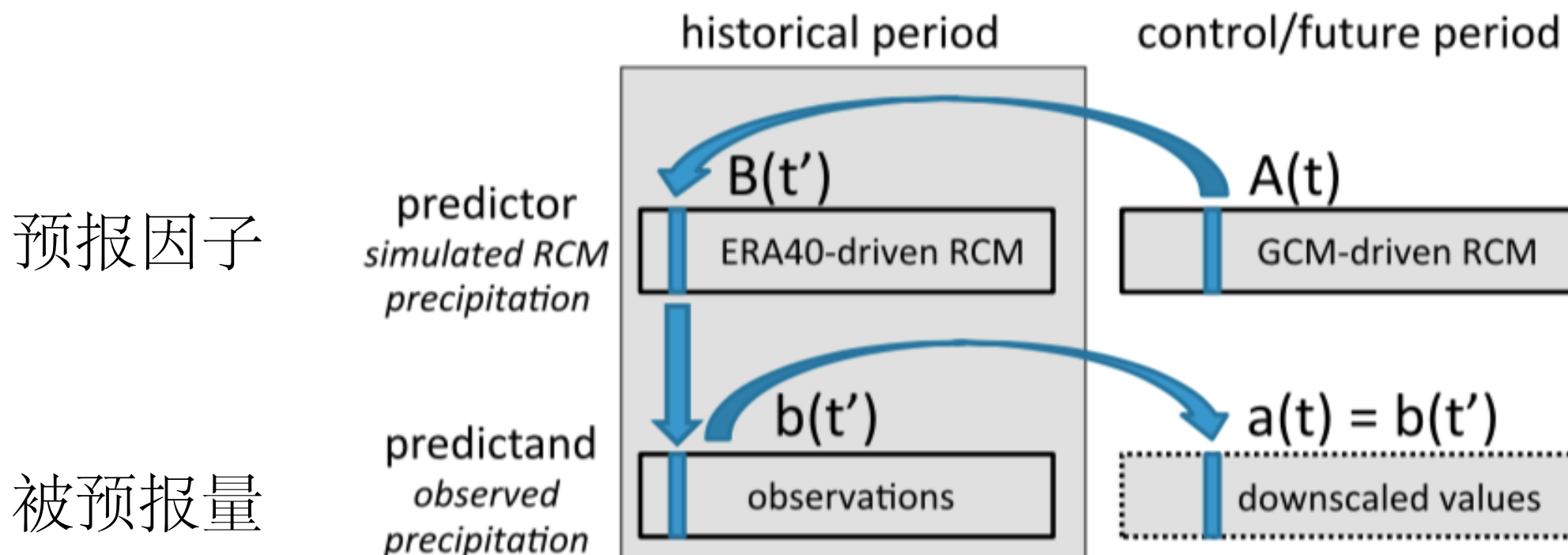


**Figure 2.** Schematic illustration of the MOS-Analog method (adapted from Fernandez and Saenz [2003]). See the text for details.

值得注意的是，该方法仅能生成在历史数据中观察到的值，因此该限制可能会影响其在未来气候变化模拟中的泛化能力，尤其是一些极端值。

# Method

## 2. Quantile Mapping Method: QQM

该方法默认观测和模拟的降水强度分布近似为gamma分布；

为了可以和MOS-Analog方法具有可比性，传递函数由ERA40驱动的模拟进行调整，并将其运用于在20C3M（历史）和未来A1B情境下校准GCM驱动的模拟：

$$X_{GCM}^* = F_{\text{Obs}}^{-1}(F_{\text{ERA40}}(X_{GCM}))$$

$X_{GCM}$ 和 $X_{GCM}^*$ 为原始的GCM驱动的模拟和被矫正过后的GCM模拟值， $F_{\text{Obs}}$ 和 $F_{\text{ERA40}}$ 为满足Gamma分布的观测和由ERA40驱动的模拟

# Method

## 3. Comparison Measures

使用三种方法来评估MOS-Analog方法的能力：

1) 同时比较观测和模拟数据在Table 2中不同变量的表现；

**Table 2.** Climatic Mean and Extreme ETCCDI Indices for Precipitation Used in This Work (See Also <http://etccdi.pacificclimate.org>)

Label	Description	Units
PRCPTOT	Total precipitation	mm
R1	Number of day with precipitation over 1 mm/d	days
SDII	Mean precipitation amount on a wet day (>1 mm)	mm
R20	Number of days with precipitation over 20 mm/d	days
RX1DAY	Maximum precipitation in 1 day	mm
CDD	Consecutive dry days (<1 mm)	days
CWD	Consecutive wet days (>1 mm)	days

# Method

## 3. Comparison Measures

- 2) 为了评估该方法 (MOS) 对年循环特征的捕捉，对Fig1中不同流域的月尺度 (1971-2000) 的表现进行评估；
- 3) 对该方法在关于保留RCMs中气候变化信号方面的表现进行评估，并和使用了经典的偏差校正方法 (QQM) 后的输出结果进行比较。

# Results

**Table 1.** RCM Simulations Produced in the ENSEMBLES Project Used in This Study With the Corresponding Driving GCM<sup>a</sup>

Number - Acronym	RCM	Driving GCM	Reference
1 - CNRM <sup>b</sup>	ALADIN	ARPEGE	<i>Radu et al. [2008]</i>
2 - DMI <sup>b</sup>	HIRHAM	ARPEGE	<i>Christensen et al. [2008]</i>
3 - DMI-BCM	HIRHAM	BCM	<i>Christensen et al. [2008]</i>
4 - DMI-ECHAM5	HIRHAM	ECHAM5-r3	<i>Christensen et al. [2008]</i>
5 - ICTP <sup>b</sup>	RegCM3	ECHAM5-r3	<i>Pal et al. [2007]</i>
6 - KNMI <sup>b</sup>	RACMO	ECHAM5-r3	<i>Van Meijgaard et al. [2008]</i>
7 - HC <sup>b</sup>	HadRM3Q0	HadCM3Q0	<i>Haugen and Haakensatd [2006]</i>
8 - MPI <sup>b</sup>	M-REMO	ECHAM5-r3	<i>Jacob [2001]</i>
9 - SMHI <sup>b</sup>	RCA	ECHAM5-r3	<i>Samuelsson et al. [2011]</i>
10 - SMHI-BCM	RCA	BCM	<i>Samuelsson et al. [2011]</i>

<sup>a</sup>The numbers are used to facilitate the reading of the Taylor diagrams presented later (see section 4).

<sup>b</sup>The best performing models in this region according to previous studies [*Herrera et al., 2010; Turco et al., 2013*].

# Results

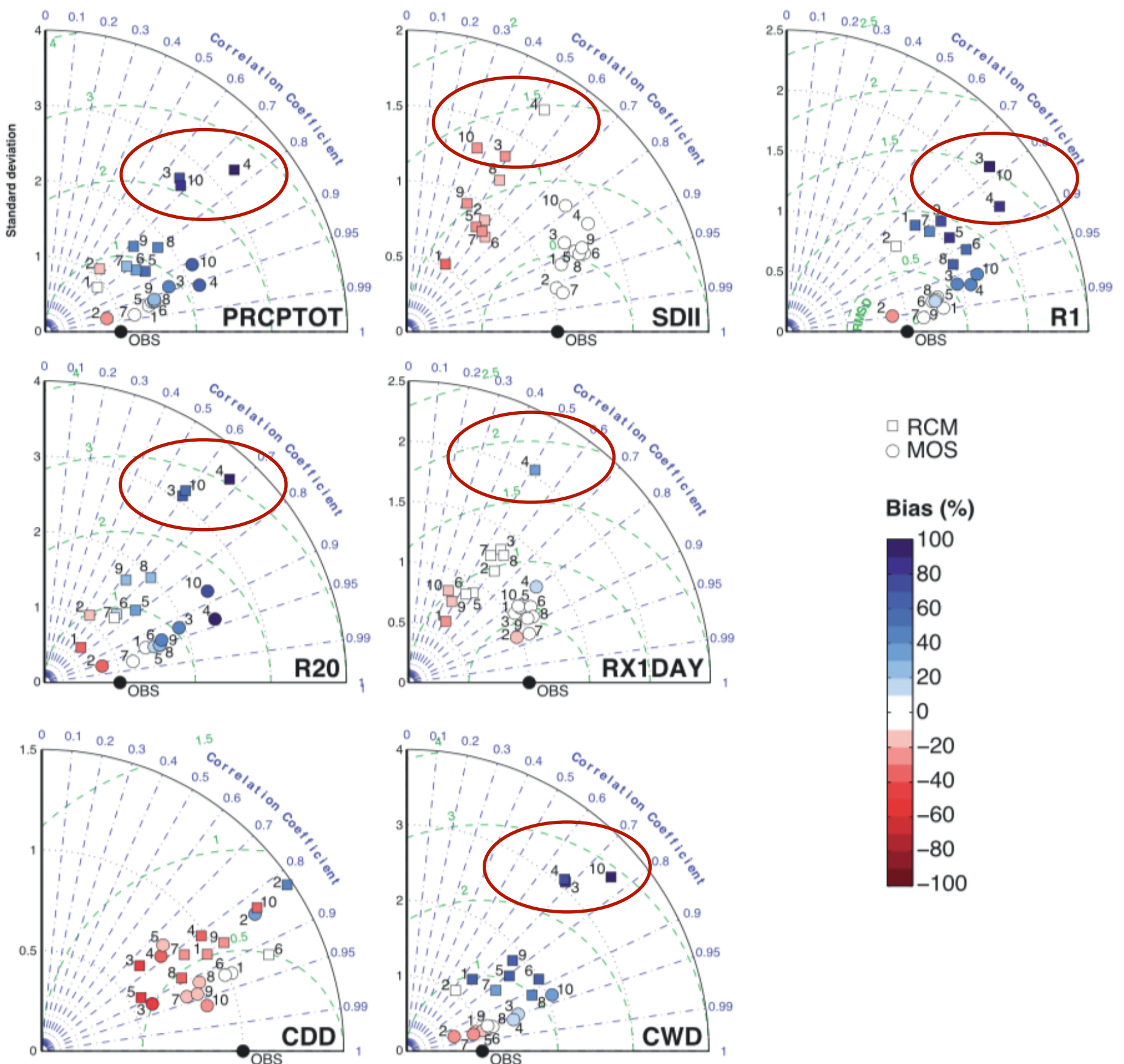


**Figure 4.** Taylor diagrams for the GCM-driven RCMs for different ETCCDI indices (Table 2). The squares and the dots with the numbers indicate, respectively, the model output (as referred on Table 1) and the MOS-Analog applied to this model.

# Results

**Table 1.** RCM Simulations Produced in the ENSEMBLES Project Used in This Study With the Corresponding Driving GCM<sup>a</sup>

Number - Acronym	RCM	Driving GCM	Reference
1 - CNRM <sup>b</sup>	ALADIN	ARPEGE	<i>Radu et al. [2008]</i>
2 - DMI <sup>b</sup>	HIRHAM	ARPEGE	<i>Christensen et al. [2008]</i>
3 - DMI-BCM	HIRHAM	BCM	<i>Christensen et al. [2008]</i>
4 - DMI-ECHAM5	HIRHAM	ECHAM5-r3	<i>Christensen et al. [2008]</i>
5 - ICTP <sup>b</sup>	RegCM3	ECHAM5-r3	<i>Pal et al. [2007]</i>
6 - KNMI <sup>b</sup>	RACMO	ECHAM5-r3	<i>Van Meijgaard et al. [2008]</i>
7 - HC <sup>b</sup>	HadRM3Q0	HadCM3Q0	<i>Haugen and Haakensatd [2006]</i>
8 - MPI <sup>b</sup>	M-REMO	ECHAM5-r3	<i>Jacob [2001]</i>
9 - SMHI <sup>b</sup>	RCA	ECHAM5-r3	<i>Samuelsson et al. [2011]</i>
10 - SMHI-BCM	RCA	BCM	<i>Samuelsson et al. [2011]</i>

<sup>a</sup>The numbers are used to facilitate the reading of the Taylor diagrams presented later (see section 4).

<sup>b</sup>The best performing models in this region according to previous studies [*Herrera et al., 2010; Turco et al., 2013*].

筛选后，得到7个RCM

# Results

1. MOS-Analog 方法可以显著提升每个指数上RCM 的结果（相关系数和标准差均和观测相当）；
2. 在误差方面， MOS-Analog降尺度方法可以提升RCM的偏差和均方根误差；
3. 最重要的是，该方法明显降低了对降水频率的高估。

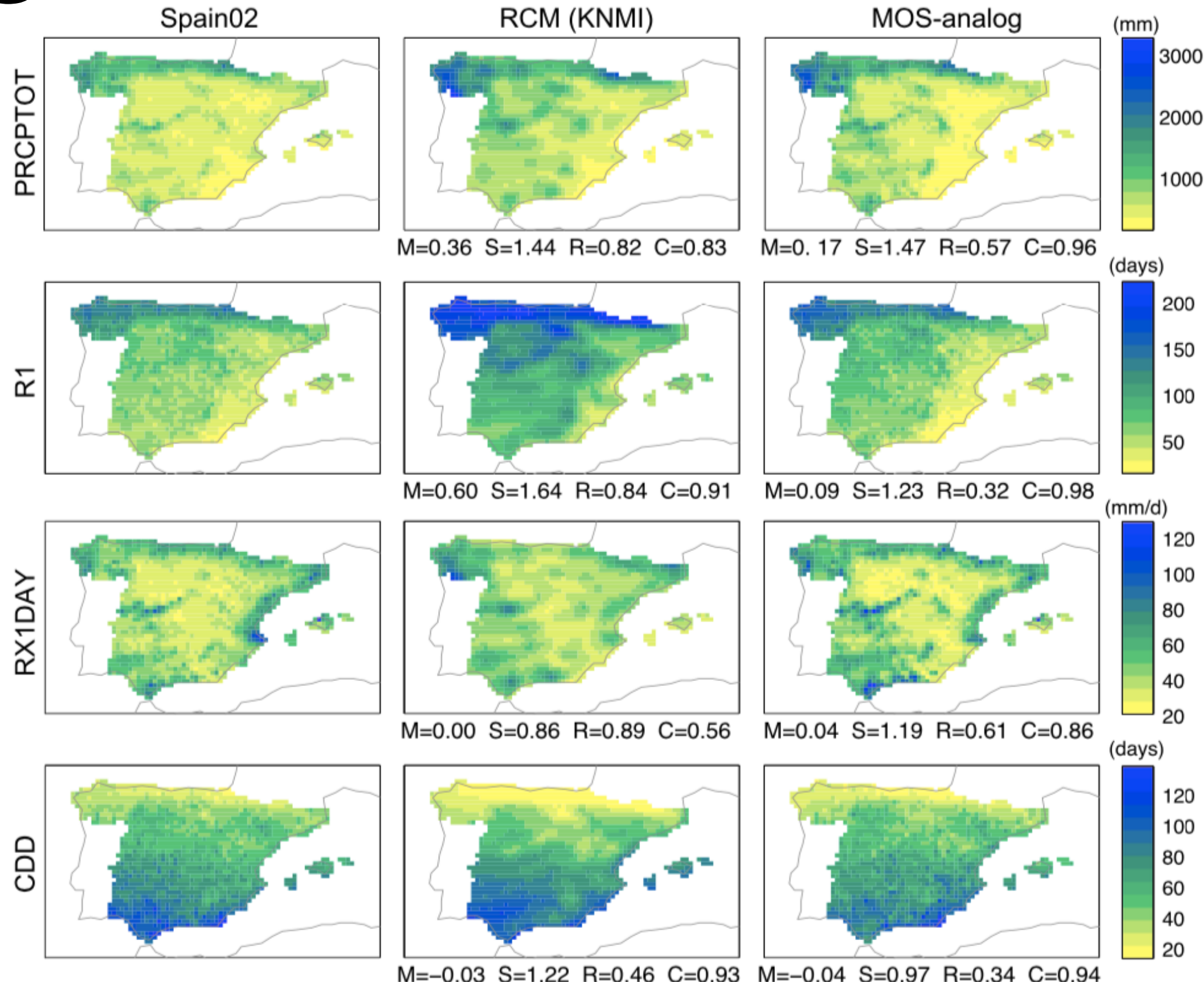


**Figure 3.** Spatial distribution of the observed (left column) Spain02, (middle column) RCM, and (right column) MOS-Analog mean values (averaged over the baseline period 1971–2000) for some of the precipitation indices shown in Table 2. The spatial validation scores for the RCM and MOS-Analog simulated values are given below the corresponding panels: mean error  $M$  (in % with respect to the observed mean); the relative standard deviation  $S$ ; the centered root-mean-square  $R$ ; and the correlation  $C$ .

# Results

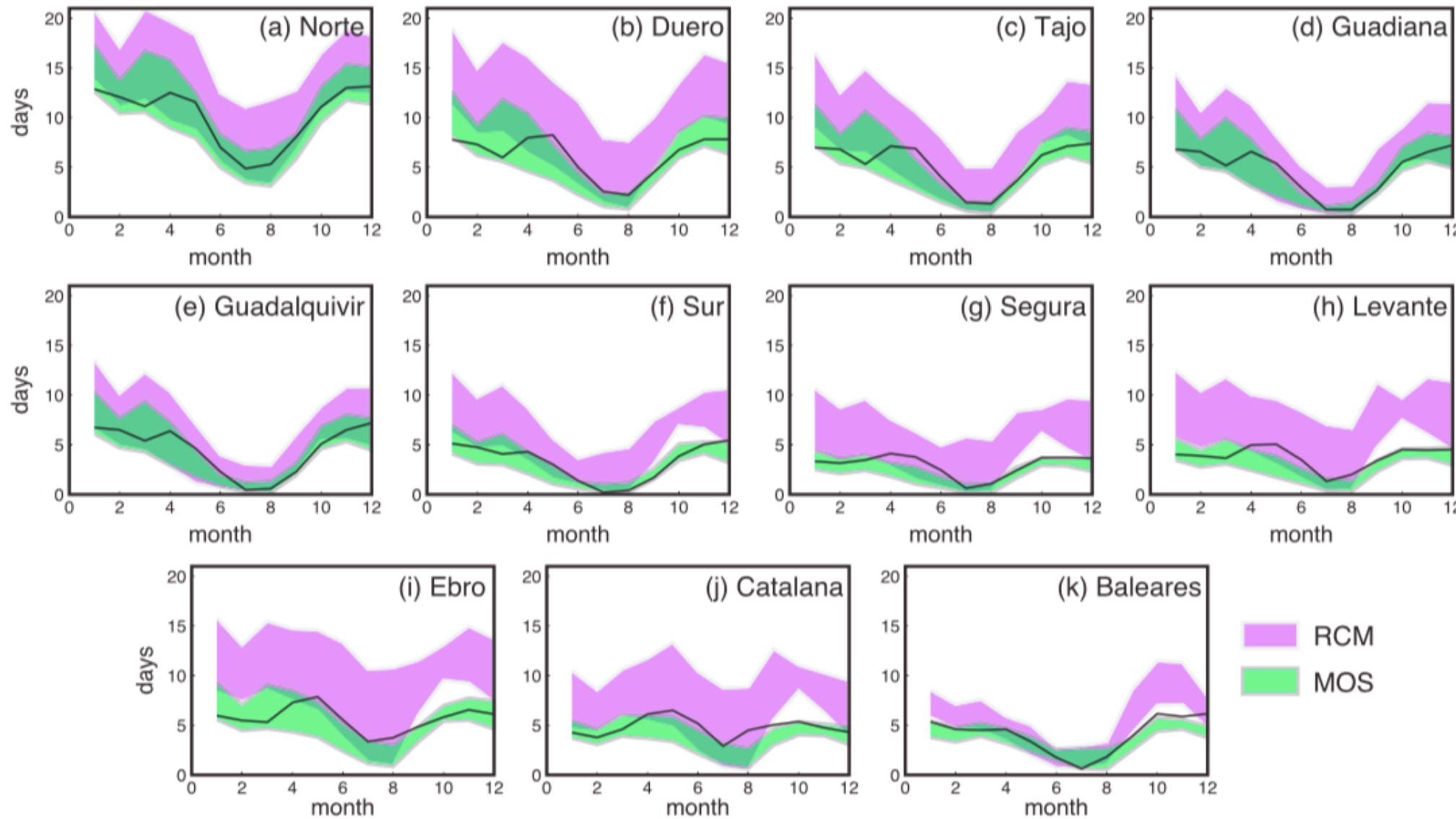


**Figure 5.** Seasonal cycle of the spatially averaged R1 index (in days) for each river basin (according to Figure 1). The black line represents the observed (Spain02) climatology. The violet-shaded band spans the values for the RCMs, while the green one spans the respective MOS downscaled values.

1. remarkable;
2. smaller uncertainty;
3. MOS-Analog 校正了RCMs 对降水的高估情况；
- 4.再现了降水变量的季节循环特征。

1. 地中海盆地一年有两个极大值，第一个极大值在秋季，第二个在春季；
2. 其他类型的盆地，最大值出现在冬季，最小值出现在夏季。

# Results

2011-2100

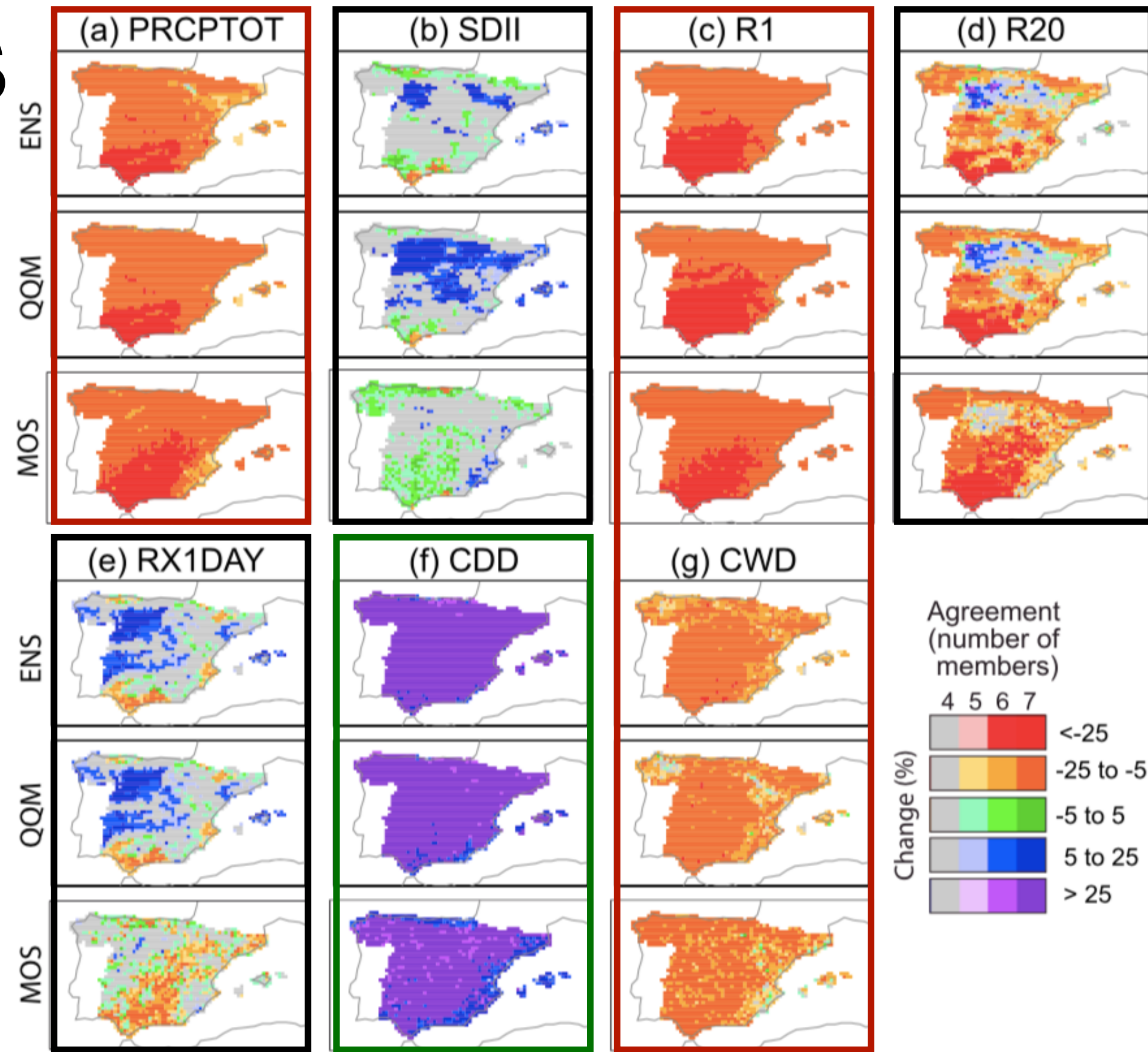


**Figure 7.** Future climate change signals (expressed as percentage of change with regard the baseline control period 1971–2000) for the period 2071–2100 for the precipitation indices shown in Table 2. The different rows correspond to the results for to the seven-member ensemble (ENS), the quantile mapping bias correction method (QQM), and the MOS-Analog downscaling method. The color saturation level shows the percentage agreement in the direction of change among the ensemble members.

# Results

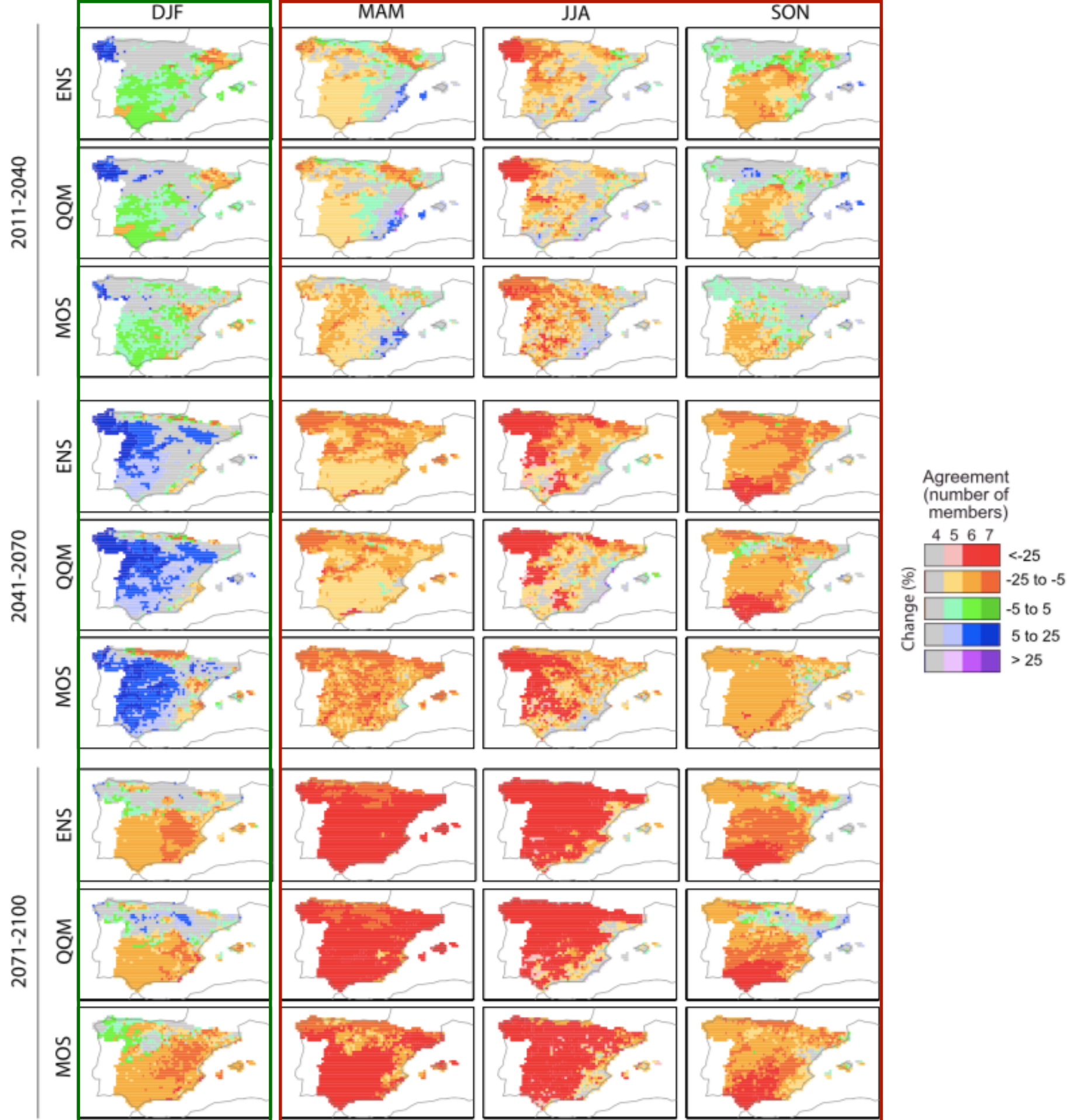


**Figure 8.** Seasonal changes of the precipitation index  $\text{PRCPTOT}$  for different future periods (2011–2040, 2041–2070, 2071–2100). Values for MOS-Analog (MOS), the quantile mapping bias correction method (QQM), and RCMs (ENS) are expressed in percentage of change between the baseline (1971–2000) and future periods. The color saturation level shows the percentage agreement in the direction of change among the ensembles.

# Conclusions

1. MOS-Analog方法明显改进了RCM原始输出的偏差；对于未来，各个变量的变化非常一致，并且具有空间上的一致性；本文的模型结果为地中海地区不断增加的干旱提供了一定可信度；
2. RCM的气候变化信号通过基于分布的分位数映射方法得到了普遍保留，而MOS-Analog方法同样也保留了其气候变化信号；
3. 在获得更好的原始模型前，偏差校正方法依旧是一个临时解决方案。

# **Bias Correction, Quantile Mapping, and Downscaling: Revisiting the Inflation Issue**

DOUGLAS MARAUN

*GEOMAR Helmholtz Centre for Ocean Research Kiel, Kiel, Germany*

(Manuscript received 21 November 2012, in final form 7 January 2013)

# Introduction

Von Storch(1999)在其文章中指出，在完美预测(perfect prognosis)统计降尺度中，通货膨胀(inflation)或相关方法的使用是没有意义的。因为不是所有小尺度变量都可以通过大尺度中的预测因子解释，局部变量的预测通常比观测得到的局部变量方差更小。

通货膨胀方法的最直接问题是会导致均方根误差变大。因此Von Storch(1999)据此提出了随机化的方法，即，增加随机的小尺度可变性(adding random small-scale variability)。

通过数值模型模拟的天气信息通常与实际情况相差巨大的系统偏差。因此对天气模型的输出做后处理以匹配观测值是十分必要的。

# Method

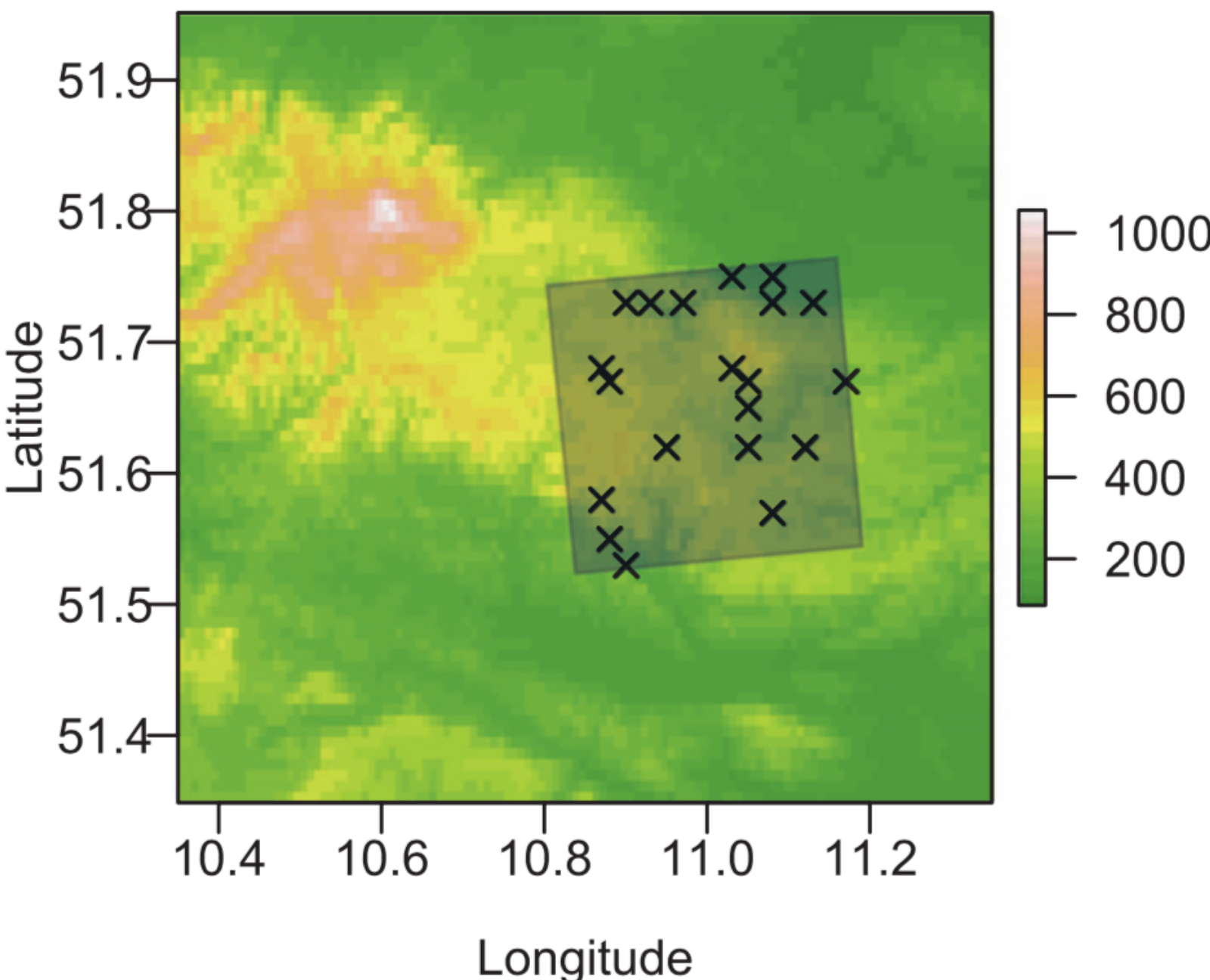


FIG. 1. Map of the Harz Mountains with the selected gauges and the RCM grid box. Elevation is given in meters above mean sea level.

以11.008N, 51.648E为中心的20个格点(Harz mountains , 德国北部);  
其中，西南部的三个格点属于Helme (河流) , 其他格点属于Bode (河流) ;  
所有河流最终汇聚于Saale, 即Elbe的支流。

# Method

TABLE 1. Chosen rain gauges. Elevation is provided in meters above mean sea level.

Gauge	Lat	Lon	Elevation	Period covered	Missing values	
					DJF	JJA
Neustadt (Talsp.)	51.58°N	10.87°E	454 m	1 Jan 1961–31 Dec 2000	0	0
Herrmannsacker	51.55°N	10.88°E	315 m	1 Jan 1961–31 Dec 2000	0	0
Stempeda	51.53°N	10.90°E	242 m	1 Jan 1969–31 Dec 2000	0	0
Hayn (Harz)	51.57°N	11.08°E	435 m	1 Jan 1961–31 Dec 2000	0	0
Strassberg	51.62°N	11.05°E	400 m	1 Jan 1969–31 Dec 2000	0	0
Harzgerode (Schee.)	51.67°N	11.17°E	250 m	1 Jun 1969–31 Dec 2000	0	0
Neudorf	51.62°N	11.12°E	425 m	1 Jan 1969–31 Dec 2000	0	0
Siptenfelde (Uhl)	51.67°N	11.05°E	412 m	1 Jun 1969–31 Dec 2000	0	0
Siptenfelde	51.65°N	11.05°E	395 m	1 Jun 1969–31 Dec 2000	0	0
Altenbrak (Talsp.)	51.73°N	10.90°E	430 m	1 Jan 1969–31 Dec 2000	0	0
Altenbrak	51.73°N	10.93°E	300 m	1 Jan 1969–31 Dec 2000	5	0
Altenbrak-Todt.	51.73°N	10.97°E	425 m	1 Jan 1969–31 Dec 2000	242	246
Hasselfelde	51.68°N	10.87°E	461 m	31 Dec 1968–31 Dec 2000	0	0
Thale (Harz)	51.75°N	11.03°E	157 m	1 Jan 1969–31 Dec 2000	31	31
Neinstedt	51.75°N	11.08°E	140 m	1 Jan 1969–31 Dec 2000	0	0
Stiege	51.67°N	10.88°E	494 m	1 Jan 1961–31 Dec 2000	181	184
Friedrichsbrunn	51.68°N	11.03°E	523 m	31 Dec 1968–31 Dec 2000	0	0
Stecklenberg	51.73°N	11.08°E	160 m	1 Jan 1969–31 Dec 1999	0	0
Gernrode	51.73°N	11.13°E	210 m	1 Jan 1961–31 Dec 2000	182	184
Breitenstein	51.62°N	10.95°E	466 m	1 Jan 1969–31 Dec 2000	0	0

# Method

1. ENSEMBLES(Ensemble-Based predictions of Climate Changes and their Impacts) project

Regional Model(REMO) from the Max Planck Institute of Meteorology(Jacob, 2001)——观测?

the RCM is driven by 40-yr European Centre for Medium-Range Weather Forecasts(ECMWF)——模式

2. Time Period: 1969-2000

# Results

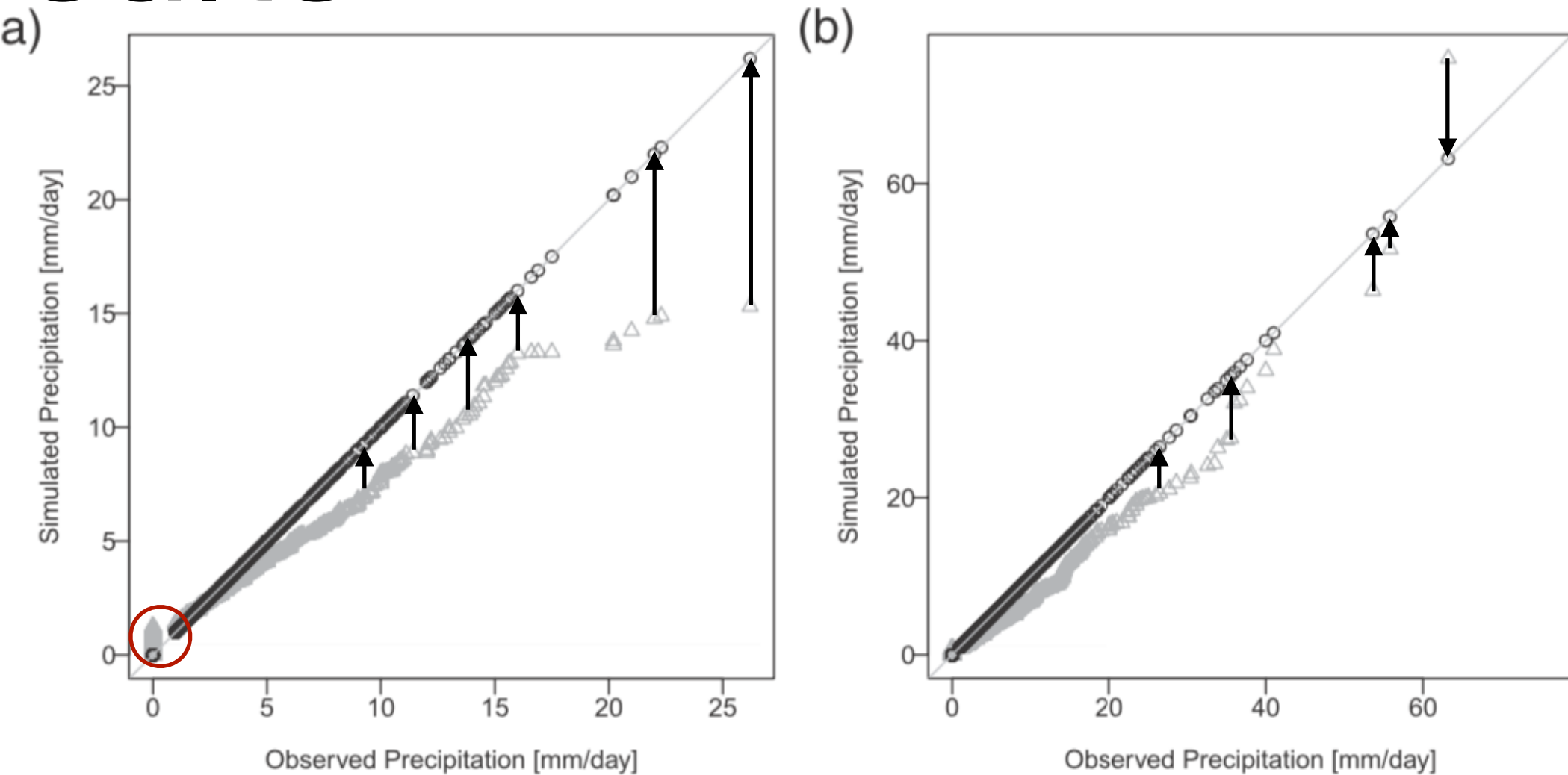


FIG. 2. Q–Q plot for Thale (Harz). Uncorrected (gray triangles) and corrected (black circles) simulated daily precipitation against observed daily precipitation: (a) December–February (DJF) and (b) June–August (JJA).

1. 冬季，未校正的RCM严重低估了观测的降水，却又产生了很多“毛毛雨”天(一定程度上是因为观测点和区域平均模拟间的尺度不匹配);
2. 夏季和冬季有相同情况，尽管RCM产生了一些降水高值可以和观测对应;
3. 两个案例中，被校正的RCM完美重现了观测降水的边缘化分布？

# Results

1. 一方面，校正后极端事件会覆盖整个网格区域，这表明分位数映射会将空间范围严重夸大；
2. 另一方面，“毛毛雨”效果被过度校正，因此网格中会出现太多完全干燥的天数。

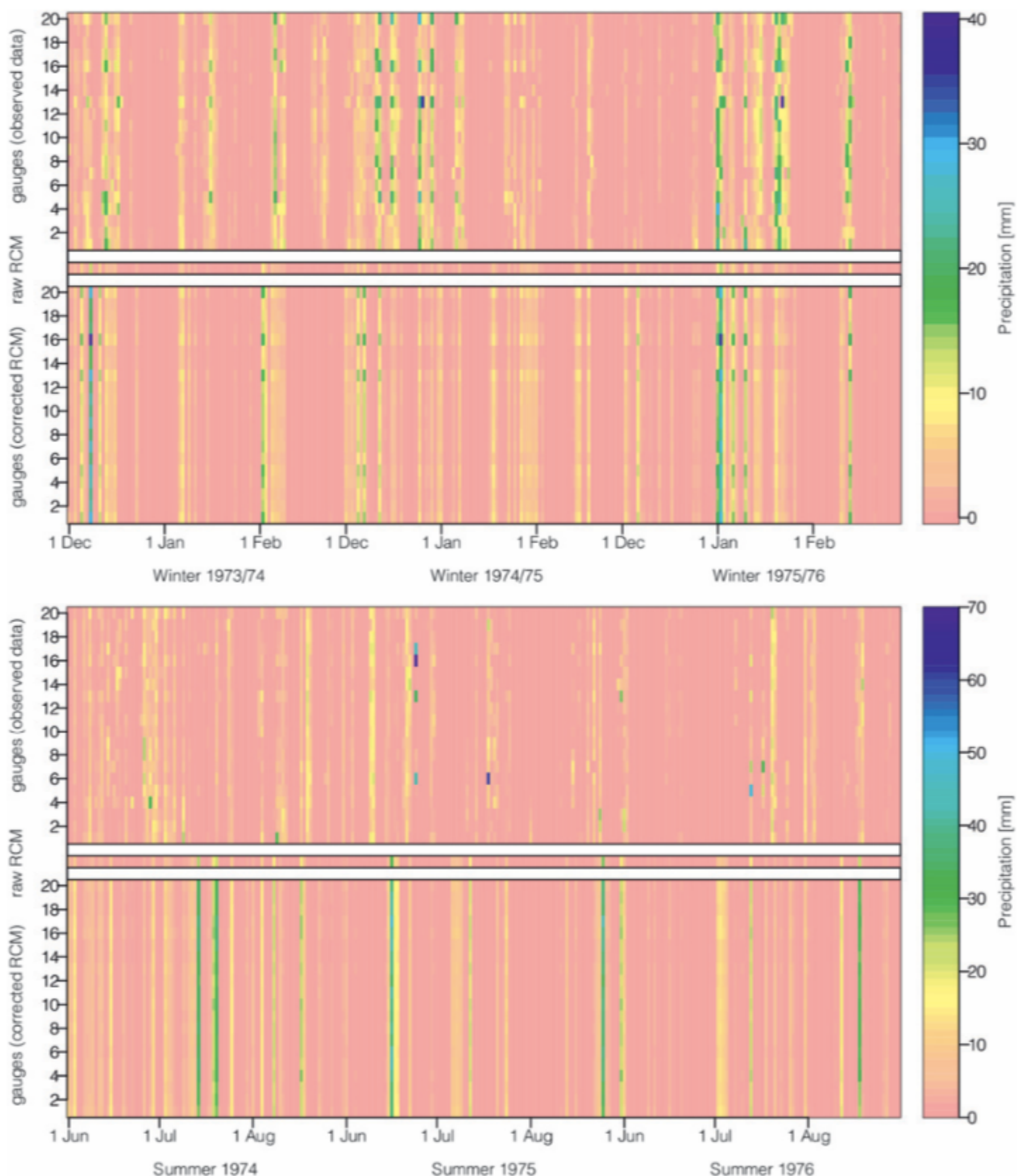


FIG. 3. Time series for selected seasons: (top) DJF and (bottom) JJA.

# Results

1. 对于冬季和夏季，“毛毛雨”效应的过度校正以及极端事件的夸大变得更为明显；
2. 校正后的模型可以模拟出过多区域平均的干燥天气，其严重将区域平均中极端事件高估了30%。

20个格点通过QM矫正后的平均值

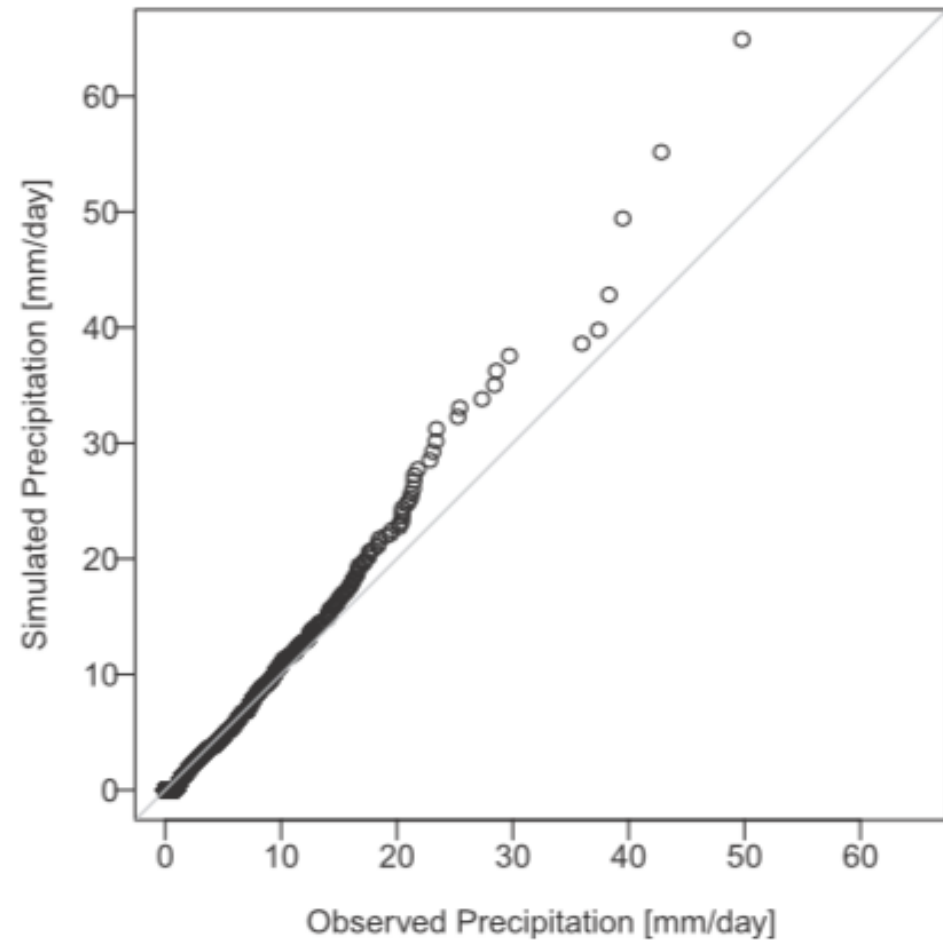
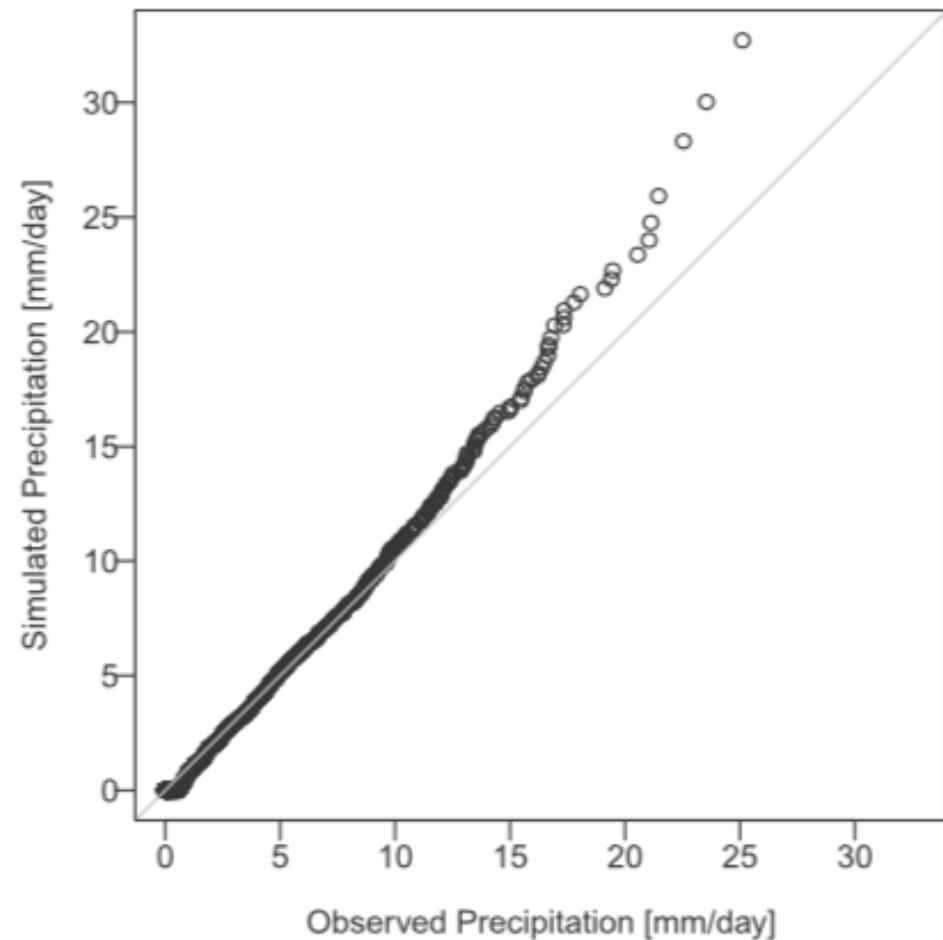


FIG. 4. Q–Q plot of area-mean precipitation for the chosen grid box. Corrected simulated daily precipitation against observed daily precipitation: (top) DJF and (bottom) JJA.

# Results

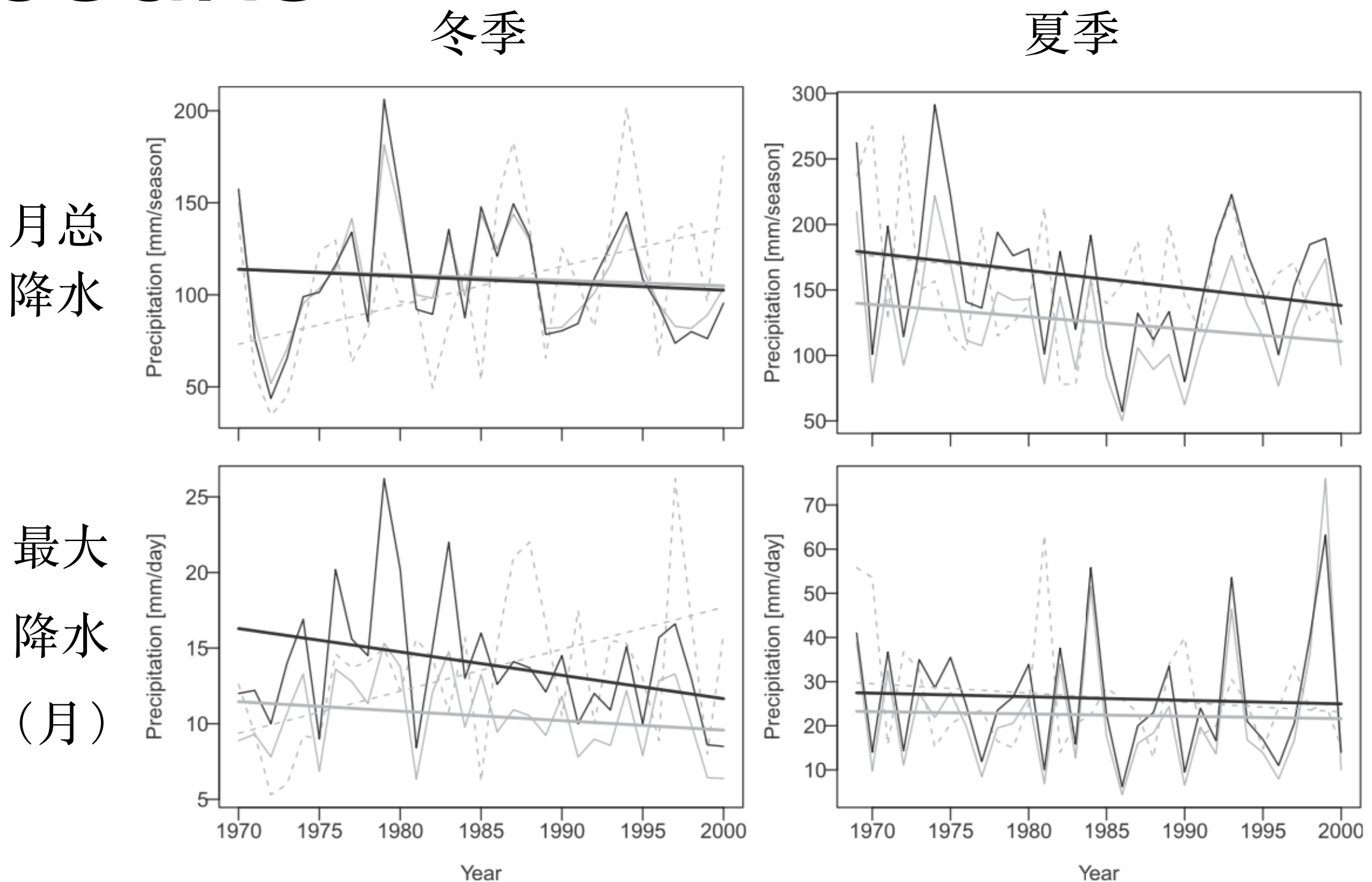


FIG. 5. Precipitation time series and trends for Thale (Harz): (top) seasonal total and (bottom) seasonal maxima for (left) DJF and (right) JJA. Dashed gray lines are observations, solid gray lines are uncorrected precipitation simulations, and black lines are corrected precipitation simulations.

# Conclusions

1. 由于分位数映射无法引入任何小尺度可变性，因此局地尺度的时间特征依旧是大网格的特征，这意味着在时间结构十分重要的特定应用中，最终结果很可能是错误的；
2. 当用于为分布式水文模型提供局地尺度的输入数据时，洪水风险[flood risk]（特别是对于快速响应的小流域）可能被严重高估；
3. 作为一系列影响，对于未来平均降水和极端降水的改变，以及任何相关影响很有可能是错误的；
4. 以上都表明对降水进行分位数映射方法是无法修正模型和观测间的偏差的，因此引入随机的偏差校正至关重要。

# Statistical downscaling of general circulation model outputs to precipitation – part 1: calibration and validation

D. A. Sachindra,<sup>a\*</sup> F. Huang,<sup>a</sup> A. Barton<sup>a,b</sup> and B. J. C. Perera<sup>a</sup>

<sup>a</sup> College of Engineering and Science, Footscray Park Campus, Victoria University, Melbourne, Australia

<sup>b</sup> School of Science, Information Technology and Engineering, University of Ballarat, Victoria, Australia

# Introduction

海平面上升、雪覆盖面积减少、极端降水时间、热浪和热带气旋频率的增加均被认为是气候变化的影响。

澳大利亚的维多利亚州自1997年以来遭受了严峻的旱灾，直到2010年年底和2011年年初时的大规模降水才得以缓解。澳大利亚西南部的干早在结束时并无任何征兆，人们认为这是气候变化阶段性的体现(is considered to have experienced a step change in climate)。

降水变量被认为是最重要的变量之一，其对人类和动物粮食的供应、灌溉等重要环节均有重要影响。

# Method

SILO database

NCEP/NCAR monthly reanalysis data

HadCM 3 GCM for the 20th century climate experiment

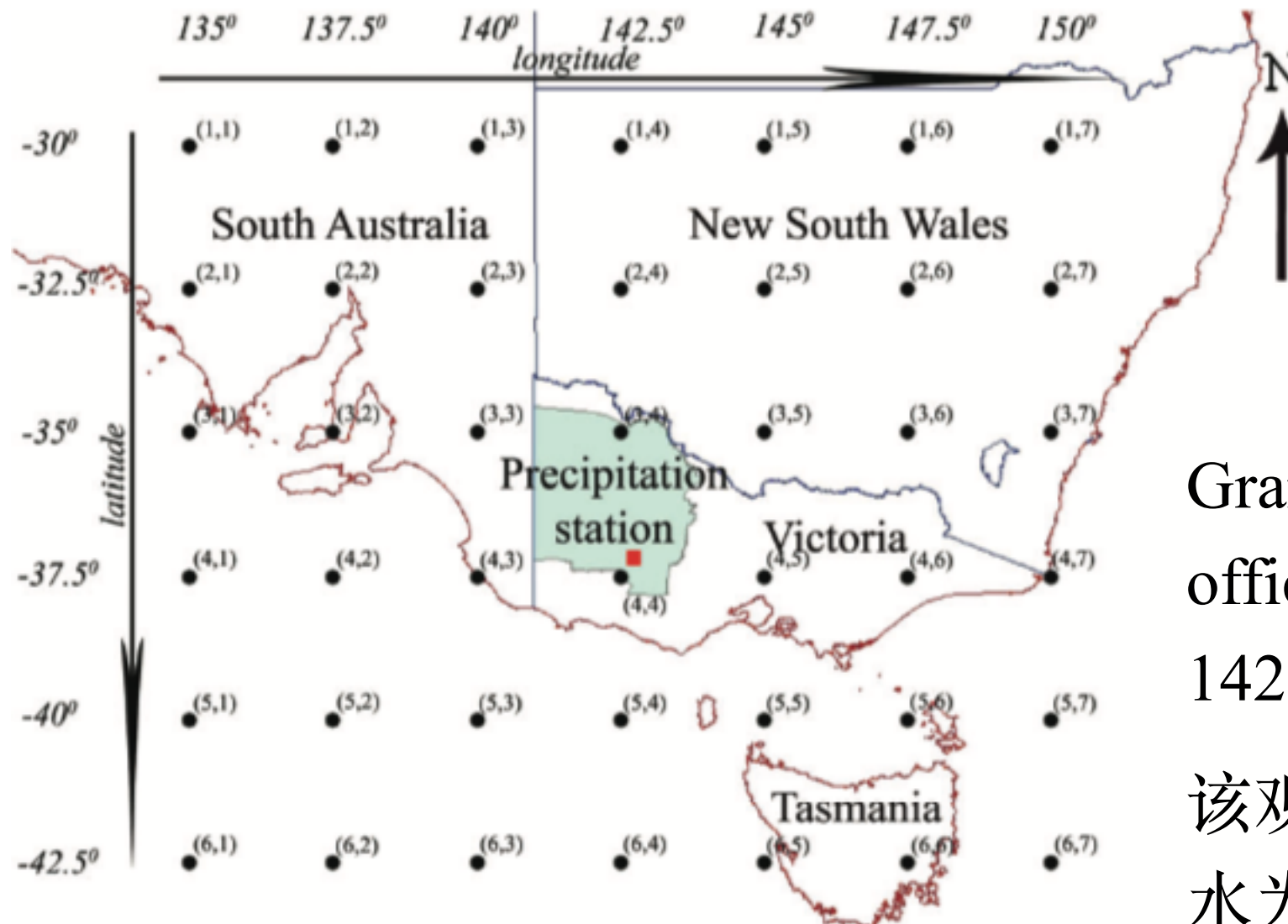


Figure 1. Atmospheric domain for downscaling.

Grampians 系统中名为 Halls Gap post office 的降水观测站 (Lat $-37.14^{\circ}$ , Lon $142.52^{\circ}$ );

该观测站在 1950-2010 间, 年平均降水为 950mm, 冬季和夏季分别为最潮湿和最干旱的季节;

# Method

Potential predictor:

200hPa, 500hPa, 700hPa, 850hPa, 1000hPa地势高度；

500hPa, 700hPa, 850hPa, 1000hPa相对湿度；

2m, 500hPa, 700hPa, 850hPa, 1000hPa比湿；

2m, 500hPa, 700hPa, 850hPa, 1000hPa温度；

地表温度； 地表气压；

平均海平面气压； 地表降水速率；

850hPa纬向风、经向风。

在1950-1969, 1970-1989, 1990-2010以及1950-2010时间片、逐月对上述变量进行Pearson相关系数计算，置信度大于95%的变量被选中。

# Results

1. 地表降水速率被认为是研究降水的最具代表的变量（列表中除7月不包含，其余月份均包含）；湿度变量（相对湿度和比湿）是大气水汽的代表性变量（12个月中有7个月均包含[February, March, May, September, October, November, December]）；
2. 在7月中，被选中的变量仅有风速和850hPa地势高度——这表明这些变量在一定程度上也可解释降水过程；
3. 表格中被选中的格点基本围绕{4, 4}；
4. 综上，在选择变量时，不仅要考虑其和观测降水的相关性还需考虑时间尺度上的相关性。

Table 2. Final sets of potential predictors for each calendar month.

Month	Potential variables used in the model with grid locations
January	Surface precipitation rate {(3,3),(4,4)} 1000 hPa specific humidity {(3,3),(3,4),(4,4)} 850 hPa meridional wind {(2,6),(3,5),(3,6)} 850 hPa relative humidity {(1,2)} 2 m specific humidity {(3,3),(3,4)}
February	Surface precipitation rate {(3,4),(4,4),(4,5)}
March	Surface precipitation rate {(3,3),(3,4),(3,5),(4,3),(4,4),(4,5),(4,6)}
April	850 hPa relative humidity {(4,3),(4,4)} Surface precipitation rate {(4,3)}
May	Surface precipitation rate {(4,4),(5,5)} 850 hPa geopotential height {(4,3)}
June	Surface precipitation rate {(3,2),(3,3),(4,2),(4,3),(4,4),(4,5)} Mean sea level pressure {(4,3),(5,3)} 850 hPa zonal wind {(2,4)} Surface pressure{(4,3),(5,3),(5,4)}
July	850 hPa zonal wind {(1,3),(1,4)} 850 hPa geopotential height {(4,3),(4,4),(4,5)}
August	Surface precipitation rate {(4,3),(5,4),(5,5)}
September	Surface precipitation rate {(2,1),(2,2),(3,2),(3,3),(3,5),(4,2),(4,3),(4,4),(4,5)} 850 hPa relative humidity {(3,3)} 700 hPa relative humidity {(3,4)}
October	Surface precipitation rate {(3,2),(4,2),(4,3),(4,4)} 850 hPa relative humidity {(4,3)} 700 hPa geopotential height {(1,1)}
November	850 hPa relative humidity {(3,2),(3,3)} Surface precipitation rate {(4,3),(4,5)}
December	Surface precipitation rate {(2,1),(3,2),(4,3),(4,4),(5,5)} 850 hPa relative humidity {(3,2)}

hPa, atmospheric pressure in hectopascal; the locations are given within brackets (see Figure 1).

# Results

1. 该降尺度模型具有捕捉月降水特征和强度的能力。
2. 在降水较小时被高估，在降水高值区域则又被低估。

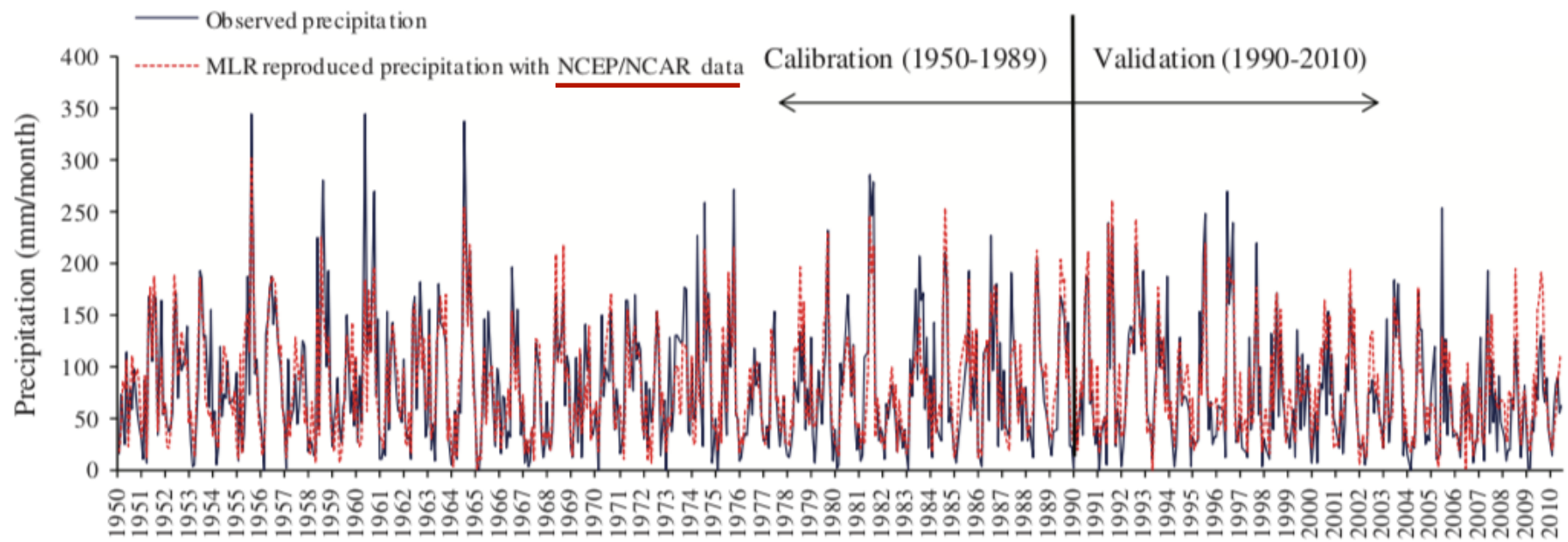


Figure 2. Observed and Model<sub>(NCEP/NCAR)</sub> reproduced monthly precipitation (1950 to 2010).

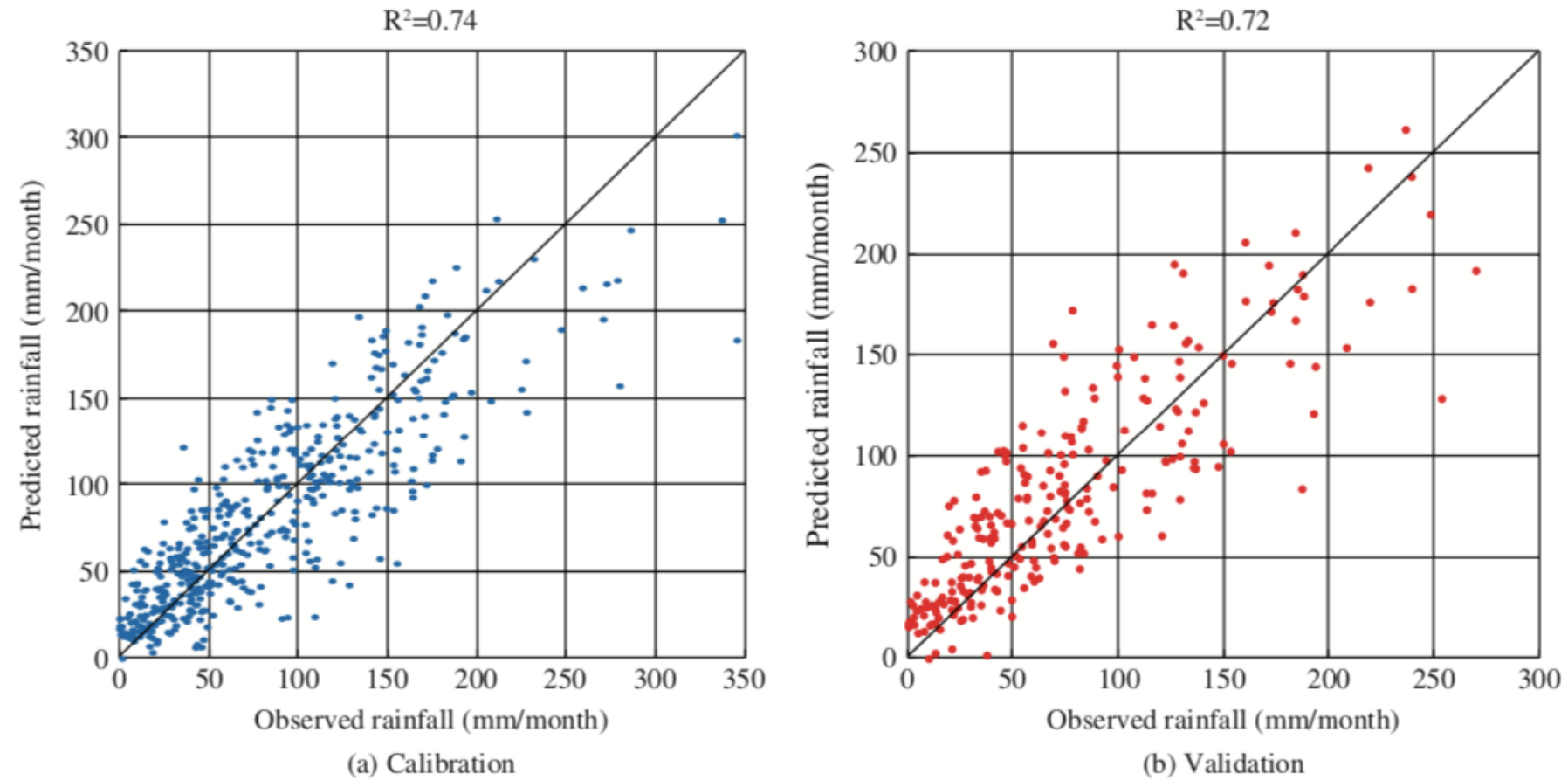
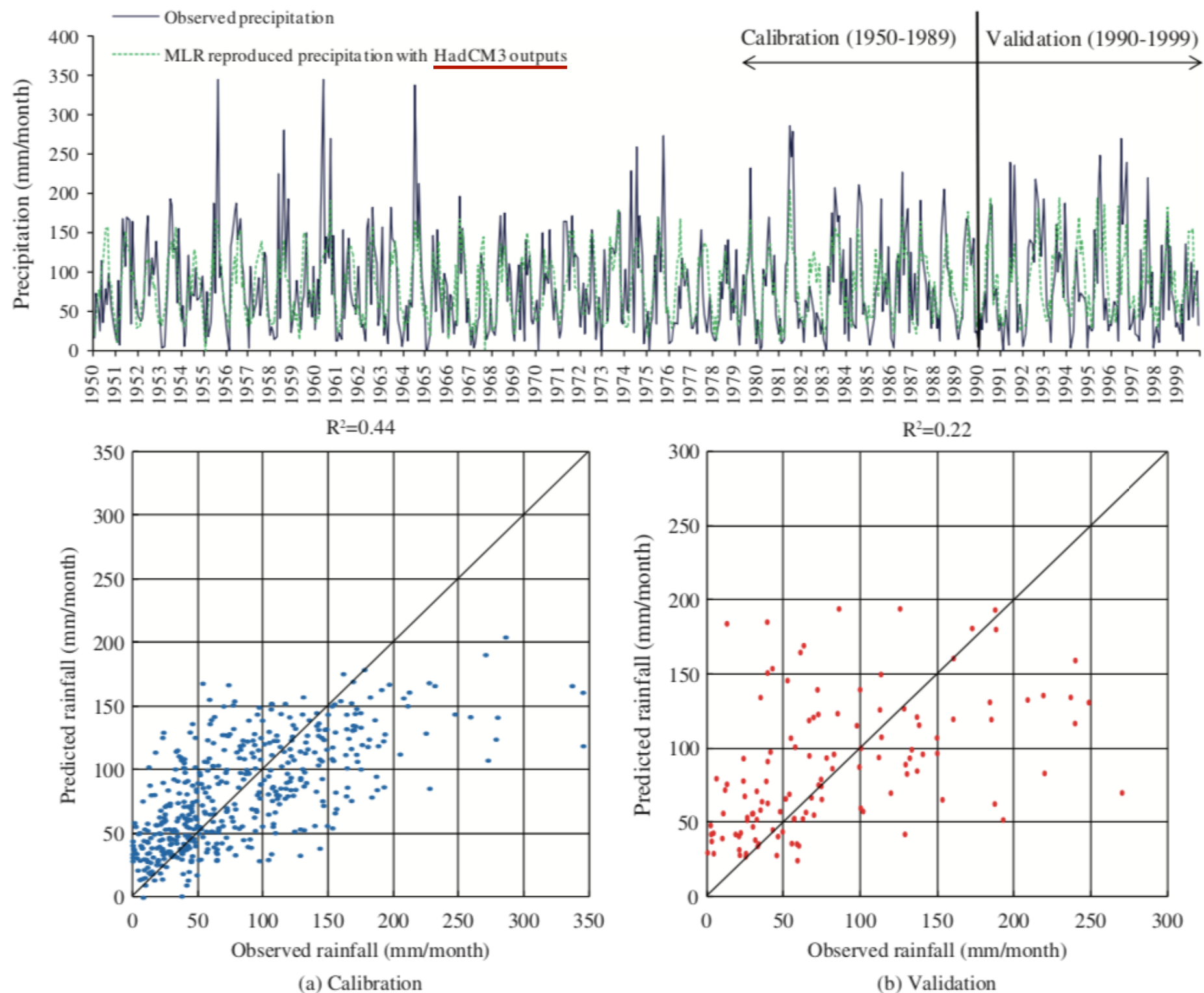


Figure 3. Scatter plots of observed and Model<sub>(NCEP/NCAR)</sub> reproduced monthly precipitation for calibration (1950–1989) and validation (1990–2010).

# Results

1. 该降尺度模型并未较好的重现降水的高值部分；
2. 并且，该模型对观测数据的再现不如使用NCEP/NCAR数据作为输出的模型好；
3. 然而，该模型还是可以大致捕捉了观测数据的降水特征；



1. 训练集和验证集中，均表现为在降水较小时被高估，在降水高值区域则又被低估；
2. 这是由于降水观测数据的方差要比GCM或再分析资料的方差大得多，因此在降尺度过程中，模型只能观测数据方差的部分，而无法表达高值和低值。

# Results

1. 两个模型在训练集和验证集均对观测的平均值捕捉的很好；
2. 然而两个模型均无法正确捕捉到观测数据的标准差和方差；
3. 相较而言，使用NCEP/NCAR数据作为输出的降尺度模型表现更好。

Table 3. Performances of downscaling models in calibration and validation.

Statistic	Calibration (1950–1989)			Validation (1990–2010)/(1990–1999) <sup>a</sup>			
	Observations	Model <sub>(NCEP/NCAR)</sub>	Model <sub>(HadCM3)</sub>	Observations		Model <sub>(NCEP/NCAR)</sub>	Model <sub>(HadCM3)</sub>
		1990–2010	1990–1999				
Avg	81.8	82.0	81.7	73.3	<b>81.8</b>	81.0	<b>87.6</b>
Std	61.7	53.2	41.1	56.9	<b>64.3</b>	51.9	<b>44.5</b>
$C_v$	0.75	0.65	0.50	0.78	<b>0.79</b>	0.64	<b>0.51</b>
NSE		0.74	0.44			0.70	<b>0.17</b>
SANS		0.66	0.26			0.61	<b>-0.20</b>
$R^2$		0.74	0.44			0.72	<b>0.22</b>

Avg, average of monthly precipitation in mm;  $C_v$ , coefficient of variation; NSE, Nash–Sutcliffe efficiency;  $R^2$ , coefficient of determination; Std, standard deviation of monthly precipitation in mm; SANS, Seasonally Adjusted Nash–Sutcliffe efficiency. <sup>a</sup>Bold italicized values in the table refer to period 1990–1999.

Table 4. Seasonal performances of downscaling models.

Model	Statistic	Calibration (1950–1989)				Validation (1990–2010)/(1990–1999) <sup>a</sup>							
		Season		Season		Summer	Autumn	Winter	Spring	Summer	Autumn	Winter	Spring
Observed		40.7	73.7	125.1	87.7	42.9/(44.3)	54.1/(57.0)	119.4/(136.1)	78.3/(89.8)				
Model <sub>(NCEP/NCAR)</sub>	Avg	40.7	73.7	125.1	87.7	49.2	57.8	132.5	85.1				
Model <sub>(HadCM3)</sub>		40.3	73.8	125.1	87.8	(44.9)	(78.8)	(128.3)	(98.5)				
Observed		33.7	58.8	64.5	53.5	41.0/(46.8)	43.1/(46.5)	61.2/(66.3)	48.4/(55.1)				
Model <sub>(NCEP/NCAR)</sub>	Std	26.0	46.6	54.1	43.9	29.8	33.1	54.1	41.7				
Model <sub>(HadCM3)</sub>		15.6	34.4	26.7	30.5	(12.7)	(39.0)	(30.0)	(42.0)				
Observed		0.83	0.80	0.52	0.61	0.96/(1.06)	0.80/(0.82)	0.51/(0.49)	0.62/(0.61)				
Model <sub>(NCEP/NCAR)</sub>	$C_v$	0.64	0.63	0.43	0.50	0.61	0.57	0.41	0.49				
Model <sub>(HadCM3)</sub>		0.39	0.47	0.21	0.35	(0.28)	(0.49)	(0.23)	(0.43)				
Model <sub>(NCEP/NCAR)</sub>	NSE	0.60	0.63	0.70	0.67	0.42	0.75	0.58	0.64				
Model <sub>(HadCM3)</sub>		0.16	0.34	0.17	0.33	(0.12)	(-0.58)	(-0.20)	(-0.15)				
Model <sub>(NCEP/NCAR)</sub>	$R^2$	0.60	0.63	0.70	0.67	0.45	0.71	0.63	0.65				
Model <sub>(HadCM3)</sub>		0.16	0.34	0.17	0.33	(0.13)	(0.04)	(0.00)	(0.09)				

Avg, average of monthly precipitation in mm;  $C_v$ , coefficient of variation; NSE, Nash–Sutcliffe efficiency;  $R^2$ , coefficient of determination; Std, standard deviation of monthly precipitation in mm. <sup>a</sup>Bold italicized values in brackets in the table refer to period 1990–1999.

# Results

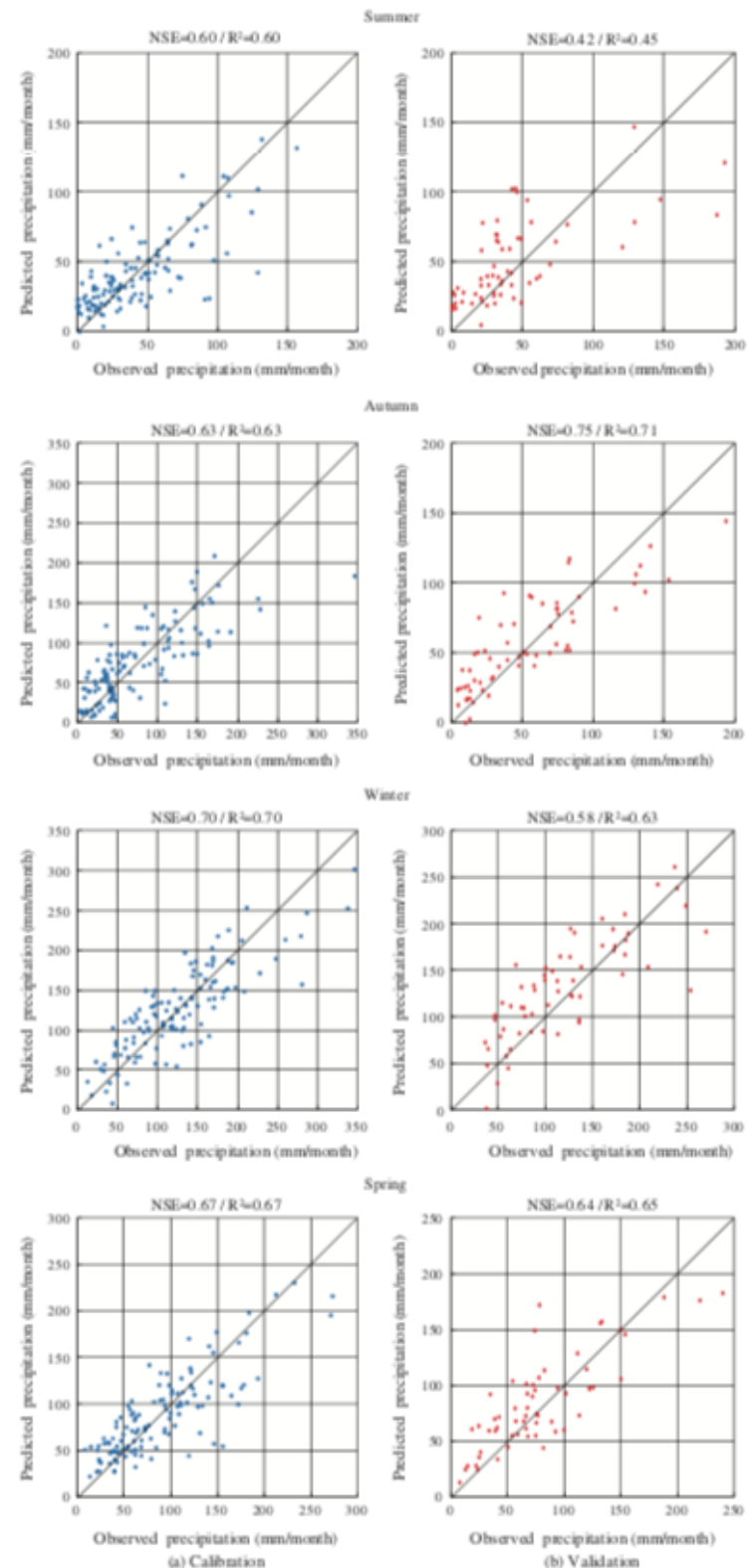


Figure 6. Seasonal scatter plots of observed and Model<sub>(NCEP/NCAR)</sub> reproduced monthly precipitation for calibration (1950–1989) and validation (1990–2010).

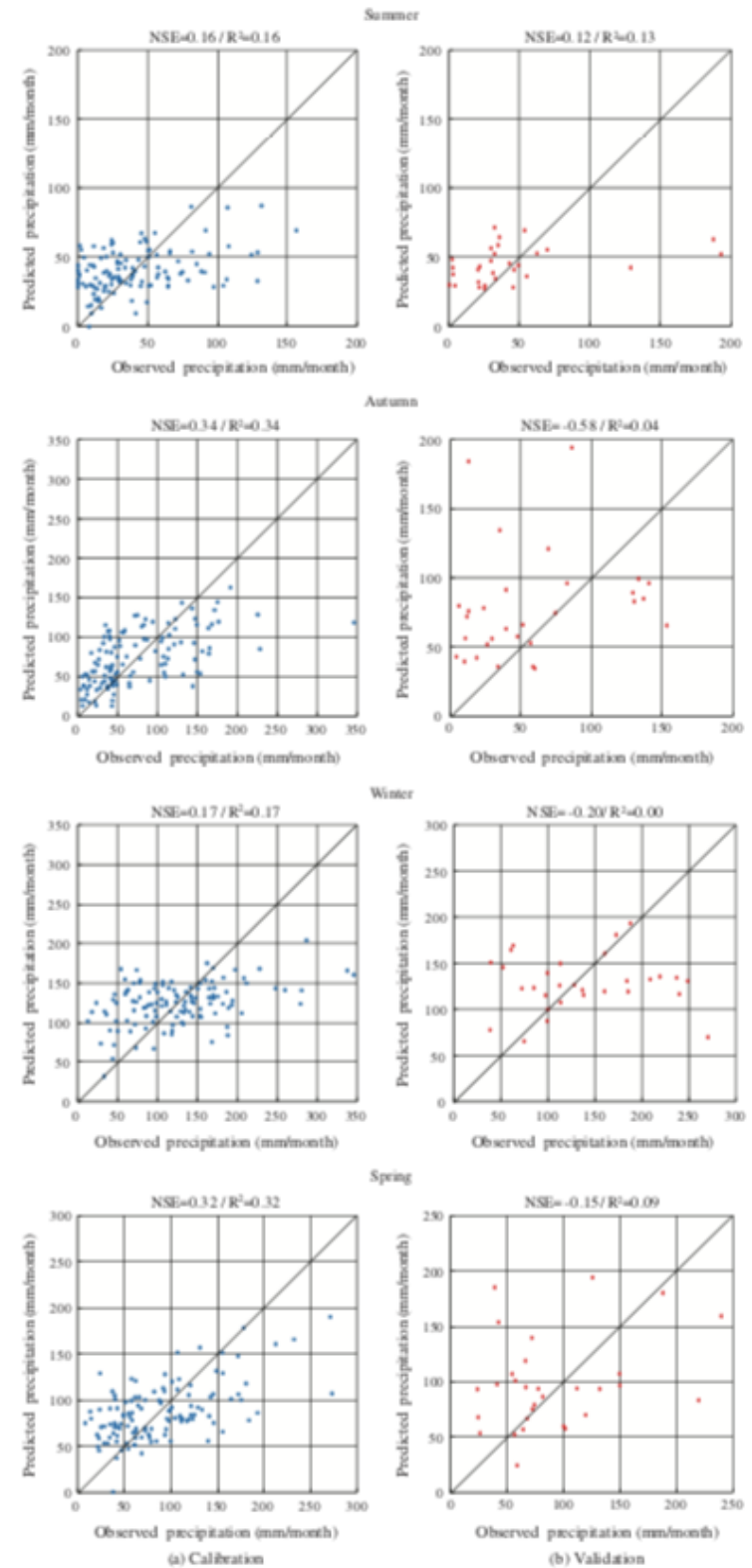


Figure 7. Seasonal scatter plots of observed and Model<sub>(HadCM3)</sub> reproduced monthly precipitation for calibration (1950–1989) and validation (1990–1999).

# Results

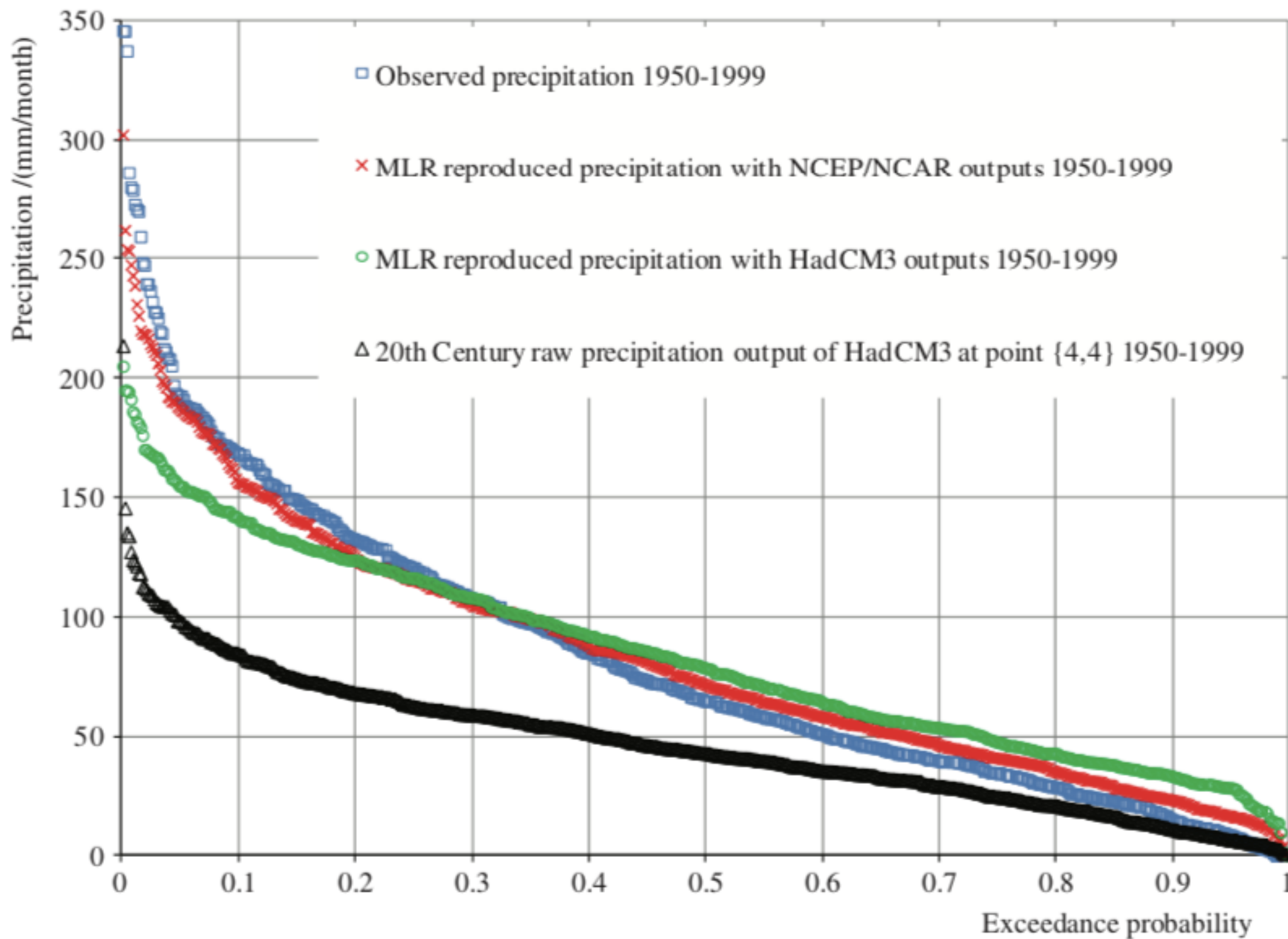


Figure 8. Precipitation probability exceedance curves (1950–1999).

# Conclusions

1. 对于全年的降水，降水速率被认为是最可用于解释观测降水数据的变量（除去7月），湿度、地势高度、平均海平面高度地表压力、和风速都在整个时间段上和观测降水变量有较高的相关性；
2. 使用NCEP/NCAR作为输出的降尺度模型在训练集和验证集上均表现良好，而使用HadCM3的模型表现较差；
3. HadCM3输出和观测数据相差较大(There was a quality mismatch between the NCEP/NCAR reanalysis and HadCM3 outputs, over the period 1950–1999)。

谢谢

# Report

2020.1.7

張慕琪

# Methods

## 实验设计：

检查——1. historical阶段， ANN得到的tmax和tmin在经过bias correction后的振幅问题。

## 绘图

地区： Beijing

时间： Train & validation

## 变量：

· Temperature:

1. Time series: CCSM, GMFD, ANN Raw, ANN(after BC);

# Time Series

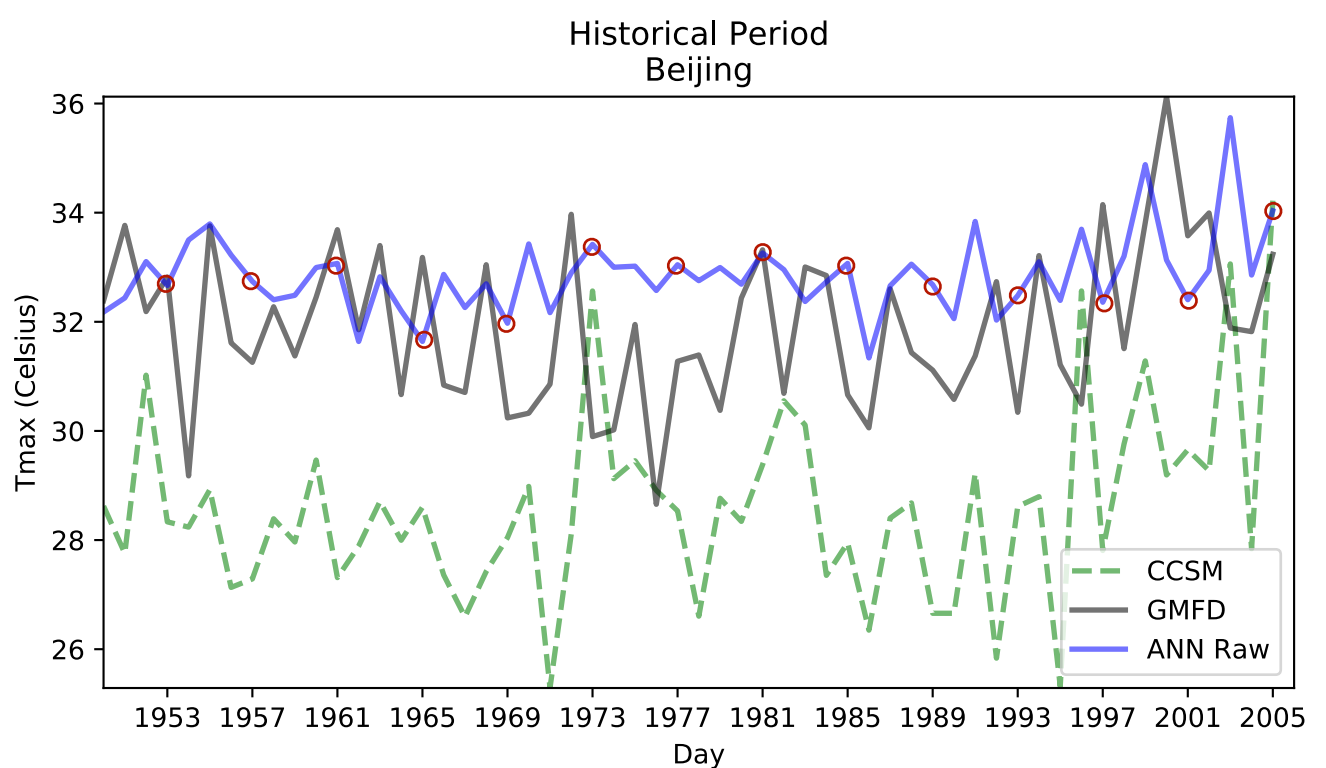
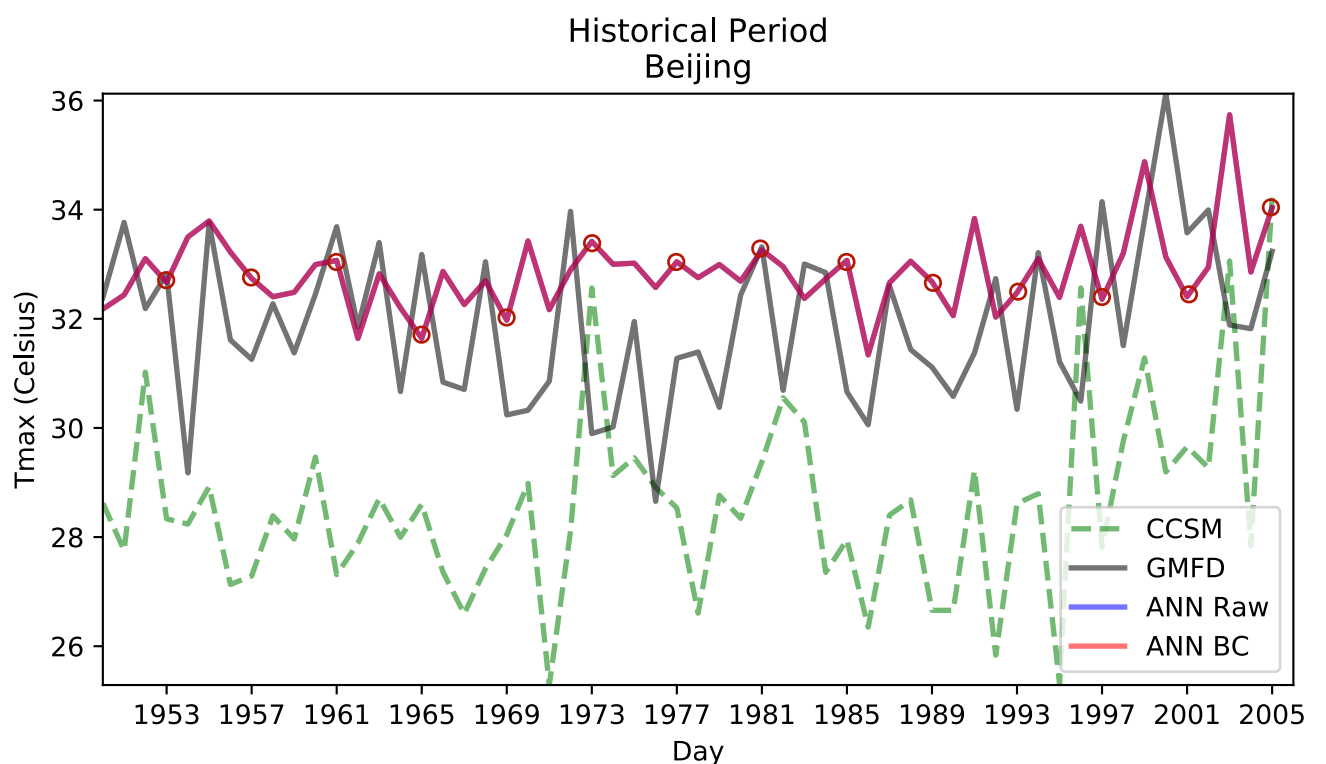
Beijing

Tmax

mean\_ccsm = 28.612423  
mean\_ann\_raw = 32.856594  
mean\_ann\_bc = 32.856598  
mean\_ground = 31.921953

std\_ccsm = 1.7578304  
std\_ann\_raw = 0.7223801  
std\_ann\_bc = 0.72237813  
std\_ground = 1.4520789

rmse\_ccsm = 3.949551  
rmse\_ann\_raw = 1.8095402  
rmse\_ann\_bc 1.8095444



谢谢

# 附录

Beijing      Tmax

mean = 264.60425

alpha = 2.3030858976500377

ann\_raw =

[264.03152 264.06384 263.94147 265.0233 265.063 264.41086 263.62625  
264.42773 264.48807 265.54465 261.83218 264.18256 262.72824 264.16983  
264.99527 264.89578 265.24808 263.68533 264.09628 264.85797 264.15036  
264.13898 264.5043 264.9275 265.13986 265.1916 264.7219 264.8386  
264.66544 266.47403 268.66724]

ann\_bc =

[263.28521729 263.35964966 263.07781982 265.56933594 265.6607666  
264.15884399 262.35183716 264.19772339 264.33666992 266.77008057  
258.21994019 263.63305664 260.28363037 263.60375977 265.50479126  
265.27566528 266.08703613 262.48791504 263.43435669 265.18859863  
263.55889893 263.53268433 264.37405396 265.34869385 265.83779907  
265.9569397 264.87518311 265.14395142 264.74517822 268.91052246  
273.96166992]

# 附录

Beijing

Tmax

```
def get_alpha(big_ann_tr, big_ground_tr):
    alpha_tmp = np.zeros((42, 12))
    alpha_new = np.zeros((12))
    for i in range(12):
        for j in range(42):
            big_ann = big_ann_tr[j, m_aa[i]:m_bb[i]].reshape(-1)
            big_ground = big_ground_tr[j, m_aa[i]:m_bb[i]].reshape(-1)
            alpha_tmp[j, i] = np.std(big_ground) / np.std(big_ann)
    alpha_new = np.mean(alpha_tmp, axis=0)
    return alpha_new

def postwork(alpha, big_ann_pr):
    big_ann = np.zeros((56, 365))
    for j in range(56):
        for i in range(12):
            mean = np.mean(big_ann_pr[j, m_aa[i]:m_bb[i]])
            big_ann[j, m_aa[i]:m_bb[i]] = ((big_ann_pr[j, m_aa[i]:m_bb[i]] - mean) * alpha[i]) + mean
    return big_ann
```